A PROBABILISTIC PRODUCTION SIMULATION APPROACH FOR SYSTEMS WITH INTEGRATED CONCENTRATED SOLAR PLANTS WITH THERMAL ENERGY STORAGE

BY

TI XU

THESIS

Submitted in partial fulfillment of the requirements
for the degree of Master of Science in Electrical and Computer Engineering
in the Graduate College of the
University of Illinois at Urbana-Champaign, 2015

Urbana, Illinois

Adviser:

Professor George Gross

ABSTRACT

The global awareness of the impacts of climate change is a key driver of the quick pace of development of renewable energy technologies. The concentrated solar plant (*CSP*) technology has emerged as a promising approach to harness solar energy, with several implementations under way around the world. Unlike *PV* and wind resources, a *CSP* allows the deployment of the thermal energy storage (*TES*), which provides the *CSP* operator the flexibility to produce electricity beyond the sunrise-to-sunset periods. For a system with integrated *CSP*s at distinct locations on its footprint, the effective utilization of the *TES* devices requires a scheduler to optimize the value of the total *CSP*-produced energy for the system. However, the assessment of impacts of *CSP* resources poses major challenges due to the inherent uncertainty, variability and intermittency of direct normal irradiation (*DNI*), which markedly influence the times and the quantities of total *CSP* energy production. The geographic correlations among the multi-site *DNI* and its intrinsic seasonality further complicate the effective quantification of the multi-site *CSP* variable effects in power systems into which they are integrated. Thus, the assessment of *CSP*s sets up an acute need for a practical simulation approach to emulate operations of the systems with integrated *CSP* resources and to evaluate their variable impacts. Such an approach must explicitly represent the uncertainty, variability and intermittency of the *CSP* resources, the geographic correlation among them, as well as the flexibility imparted by *TES* devices. The approach also needs to take into account the seasonality of the *CSP* resources and their interactions with the load seasonal changes.

To address these needs, we construct the multi-site *CSP* power output model and formulate the associated scheduling problem (*SP*) under some specific *TES* operational

objective in a system with integrated multi-site *CSP* resources. The power outputs of the multi-site *CSP*s depend not only on the specific details of the *CSP* configurations and the operational schedule, but also on the nature of the solar energy input. The identification of distinct multi-site *DNI* data in a given season is a key step to obtain the analytic representation of the multi-site *CSP* power outputs. We use statistical clustering techniques to classify the distinct data into various groups – referred to as regimes – and utilize the power output model to probabilistically characterize the multi-site *CSP* power outputs based on the identified *DNI* regimes. We make detailed use of the conditional probability concepts to incorporate the probabilistic model of the multi-site *CSP* power outputs into the extended production simulation tool.

The major interest in the use of the extended production simulation approach is to quantify the impacts of the integration of *CSP* resources into the system on the variable effects over longer-term periods. We modify the *Western Electricity Coordinating Council* (*WECC*) 240-bus model to construct a test system based on *WECC* geographic footprint, using *WECC* historical load, *DNI* and system marginal price data. We present some representative simulation results to provide insights into the multi-site *CSP* impacts on the systems over longer-term periods and to illustrate the effectiveness of the extended simulation approach.

The primary contribution of this thesis is to propose an approach capable of quantifying the variable effects of the multi-site *CSP* resources on the system into which they are integrated, with explicit representation of the uncertainty, variability and intermittency of the solar resources as well as their interactions with the loads and other resources.

For my family

ACKNOWLEDGMENTS

I would like to acknowledge the advice, guidance and support from my adviser, Professor George Gross, throughout my courses and research at the University of Illinois. I also thank Professor Peter W. Sauer, Professor Thomas J. Overbye and Professor Hao Zhu, who gave me support on the completion of this thesis.

Special thanks to my dear friend, Chen Hu, with whom I spent a lot of time during the past two years. I enjoyed his continuous presence and the moments when we worked, studied and stayed together.

I would also like to thank all the power group students and staff for their help and friendship. In particular, I enjoyed the wide range of the conversation topics with Kai, Yannick, Mirat and Ada. We are always together fighting against challenges.

Finally, special thanks to my dear family without whom nothing is possible.

TABLE OF CONTENTS

1. INTRODUCTION

In this thesis, we develop a probabilistic simulation approach for systems with integrated concentrated solar plant (*CSP*) resources with thermal energy storage (*TES*) to evaluate the impacts of the multi-site *CSP* integration on the system variable effects over longer-term periods. In this introductory chapter, we present the background and motivation for this research, briefly review the current state of the art, provide an overview of our proposed methodology and outline the rest chapters of the thesis.

1.1. Background and Motivation

The growing concern over the impacts of global climate change has resulted in legislation in numerous jurisdictions to encourage the implementation of renewable resources for electricity supply so as to reduce fossil fuel energy dependence and to curtail greenhouse gas emissions. For instance, more than half the U.S. states have set ambitious goals through their *Renewable Portfolio Standards* specifying the percentage of the electricity that needs to be served by renewable resources by specific target dates [1]. The European Union has also established binding targets with the goal to derive 20 % of the total European Union energy consumption from renewable energy sources by 2020 [2]. In the solar energy technology arena, *CSP* technology has recently experienced a steady growth, with nearly 11 GW of *CSP* projects under development around the world [3]. Typically, a *CSP* utilizes mirrors with tracking systems to focus direct normal irradiation (*DNI*) to collect solar energy for conversion into thermal energy, which is used in a steam turbine or heat engine that drives a generator to produce electricity [4]. *Parabolic trough*,

Solar tower, *Dish stirling* and *Fresnel reflector* are the four common forms of the *CSP* technology [4]. Compared to the other two forms, parabolic trough and solar tower *CSP*s are widely commercially deployed around the world [5]. The parabolic trough *CSP* technology uses parabolic mirrors to concentrate solar rays onto the receivers positioned along the mirrors' focal line and the solar tower technology employs heliostats – flat mirrors with dual-axis trackers – to focus *DNI* onto a central receiver [5]. Unlike *PV* resources, *CSP* can make use only of the *DNI* – the direct component of the irradiation. Furthermore, a salient characteristic of the *CSP* technology is the deployment of the *TES* to store a fraction of the thermal energy for later conversion. Since the utilization of *TES* allows *CSP* to produce electricity beyond the sunrise-to-sunset periods and to ensure that the power outputs meet the forecasts with a better fidelity, the *TES* is a definite advantage of *CSP* over the non-dispatchable *PV* resources. The added flexibility afforded by the *TES* is a key reason for the growing interest in *CSP* [6], with the global installed capacity of around 3,500 MW [3] by the end of 2013, shown in Fig. 1.1. Spain continued to lead the world with the 2,304-MW total installed *CSP* capacity. The U.S. also installed 410 MW of *CSP* in 2013, increasing its total *CSP* capacity by more than 80 %. Other countries involved in wide commercialization of *CSP* resources include China, South Africa and Australia. Therefore, the implementation of *CSP*s triggers an acute need for a simulation tool to efficiently quantify, over longer-term periods, the variable effects of the power systems with integrated *CSP* resources sited at distinct locations.

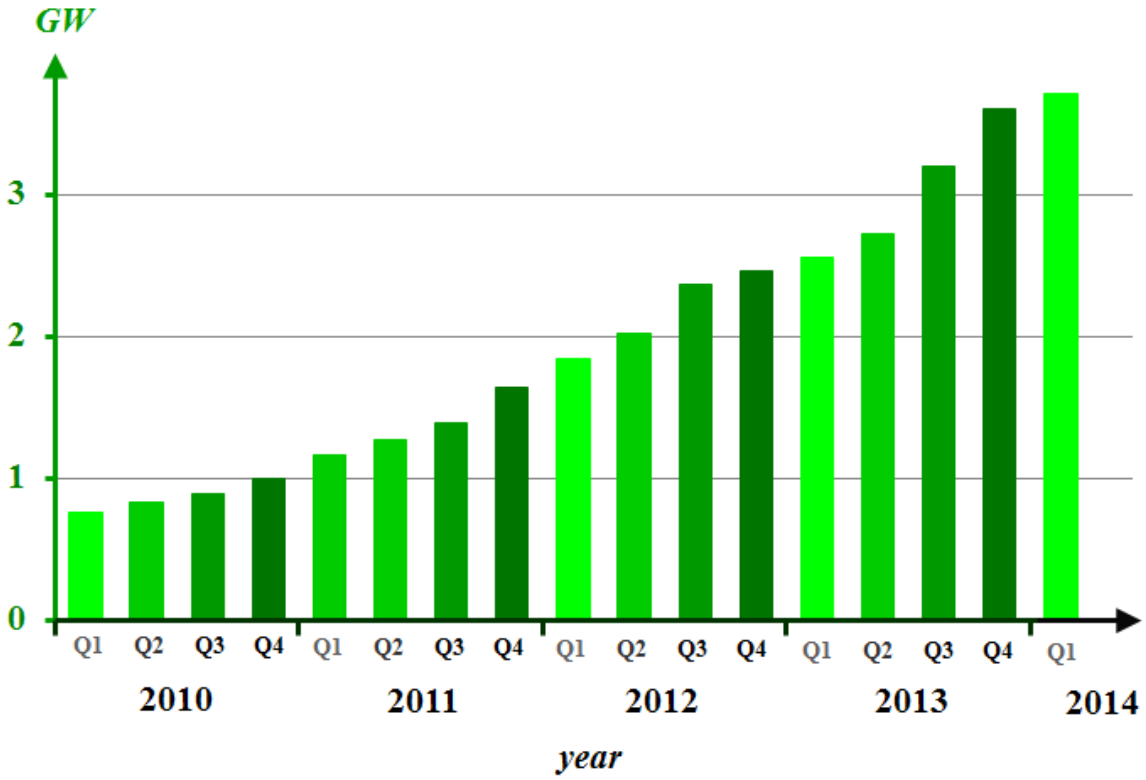

Figure 1.1: 2010 – 2014 global cumulative *CSP* capacity by quarter [3]

However, the randomness in the *CSP* resources brings major challenges into the effective assessment of the influences of the integrated multi-site *CSP*s on the systems due to the inherent uncertain, time-varying nature of the locational *DNI*s. In Fig. 1.2, we give the plots of the daily measured *DNI* data at Las Vegas, NV, for seven different days of year 2013. Clearly, the daily *DNI* shapes on May 1 and July 1 have gradual changes, whereas the shapes on Jan. 1 and Feb. 1 change rapidly from minute to minute. We show in Fig. 1.3 the variations in sunrise, sunset times and the durations of the sunrise-to-sunset periods at Ivanpah Dry Lake, CA. We note that the variations exist throughout the whole year. Based on the plot in Fig. 1.4 displaying the daily measured *DNI* data at Las Vegas, NV, and Aurora, CO, on April 7, 2014, we also notice the strong locational diversity of daily *DNI*. As a result, these characteristics of *DNI* affect markedly the times and the quantities of energy produced by the *CSP*s.

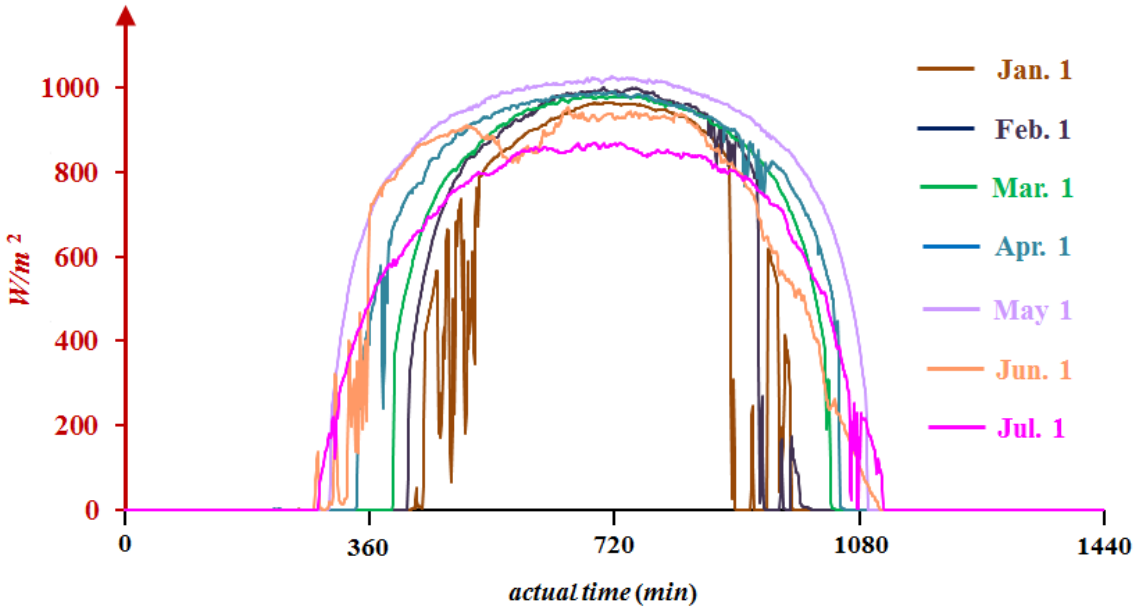

Figure 1.2: Las Vegas daily *DNI* measurements for seven different days of year 2013 [7]

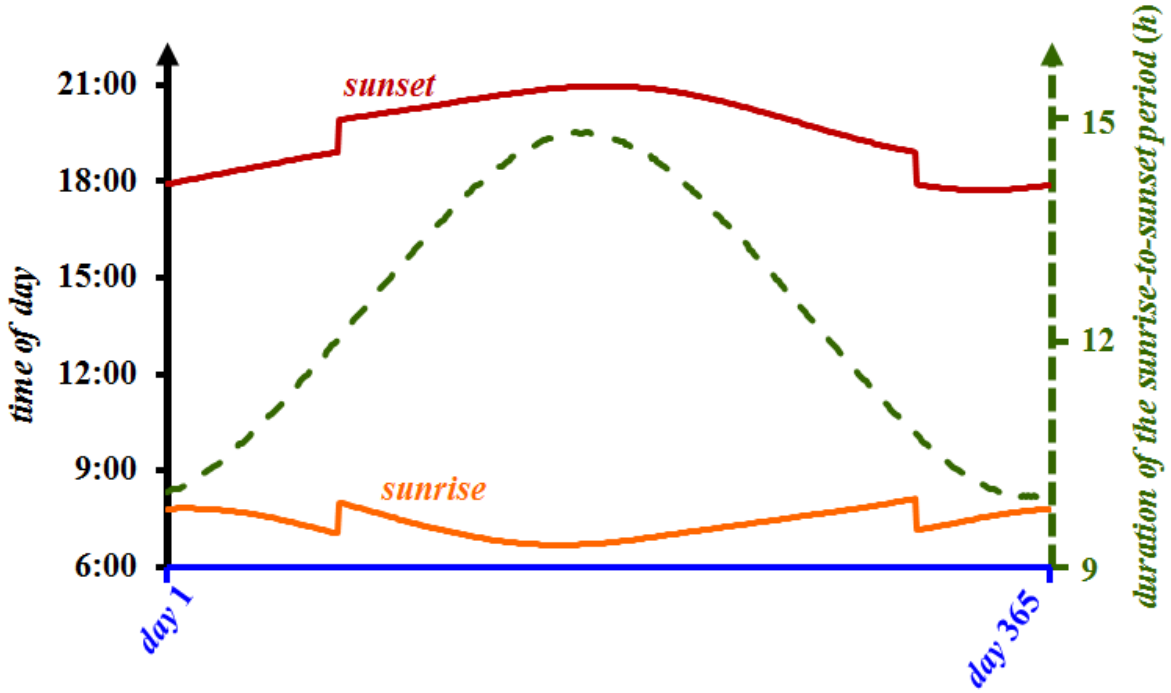

Figure 1.3: Ivanpah Dry Lake variations in sunrise/sunset times [8]

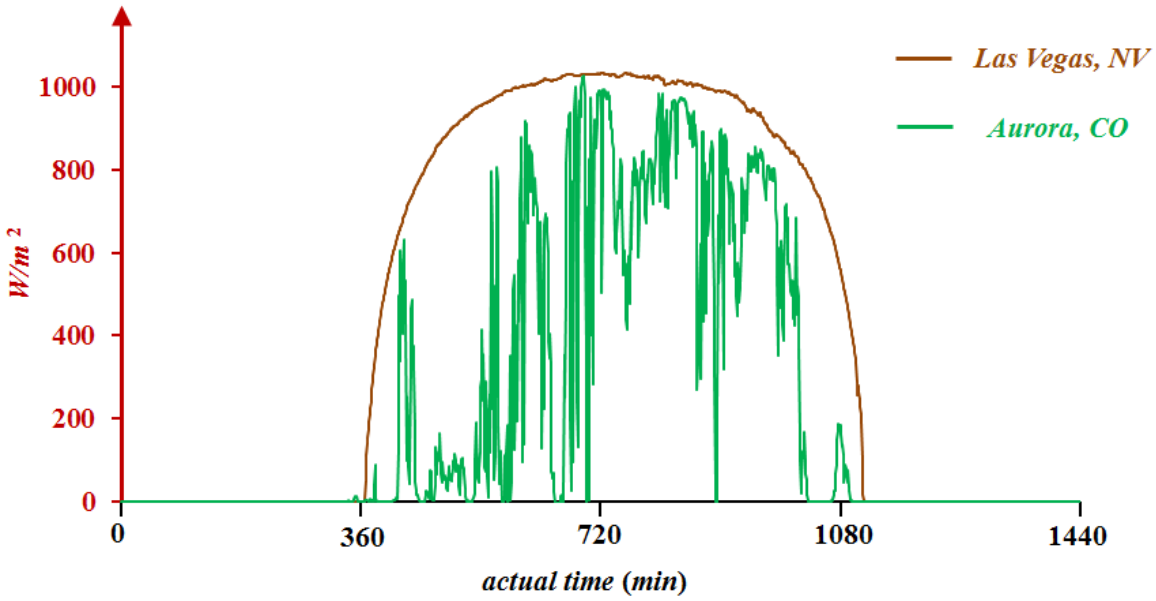

Figure 1.4: Las Vegas and Aurora daily *DNI* measurements on April 7, 2014 [3]

The *CSP* resources can output electricity whenever either solar energy or thermal energy from *TES* is available. The efficient utilization of the *TES* requires a scheduler to optimize the contribution of the *CSP*s to displace expensive and polluting conventional generation. Thus, the extent to which the aggregated *CSP* energy production and the loads are correlated is an important consideration in the evaluation of the multi-site *CSP* contribution to the power systems. In contrast to the highly uncertain, variable and intermittent *CSP* power outputs, the loads follow well-defined diurnal and weekly patterns with higher demand during the weekdays than the weekends and with peaks, typically, at similar periods of the weekdays and lower values at nights. We provide in Fig.1.5 the plots of the hourly power outputs of the *CSP*s located in *CAISO* region in comparison with the *CAISO* hourly loads [9] for March 10–16, 2014. The plots clearly indicate the weakly correlated behavior of the *CSP* outputs with the loads, which considerably impacts the multi-site *CSP* contribution to the power system where the *CSP*s are integrated. Due to the seasonality of the *DNI* and the loads, such weak correlations are also strongly seasonally

dependent, which further complicates the assessment of the *CSP* contribution. Thus, the proposed approach must be able to capture the time-varying nature of the *CSP* resources so as to effectively quantify the variable effects of systems into which they are integrated. Such a tool needs to explicitly represent the uncertainty sources in loads and resources, as well as the interactions among them. It also needs to take into account the seasonality of the loads and *CSP* resources, in addition to the *TES* operation scheduling and its impacts on *CSP* outputs. In this thesis, we address those needs with the extension of the conventional probabilistic simulation approach to construct a practical and versatile simulation tool to emulate the operations of the power systems with integrated *CSP* resources.

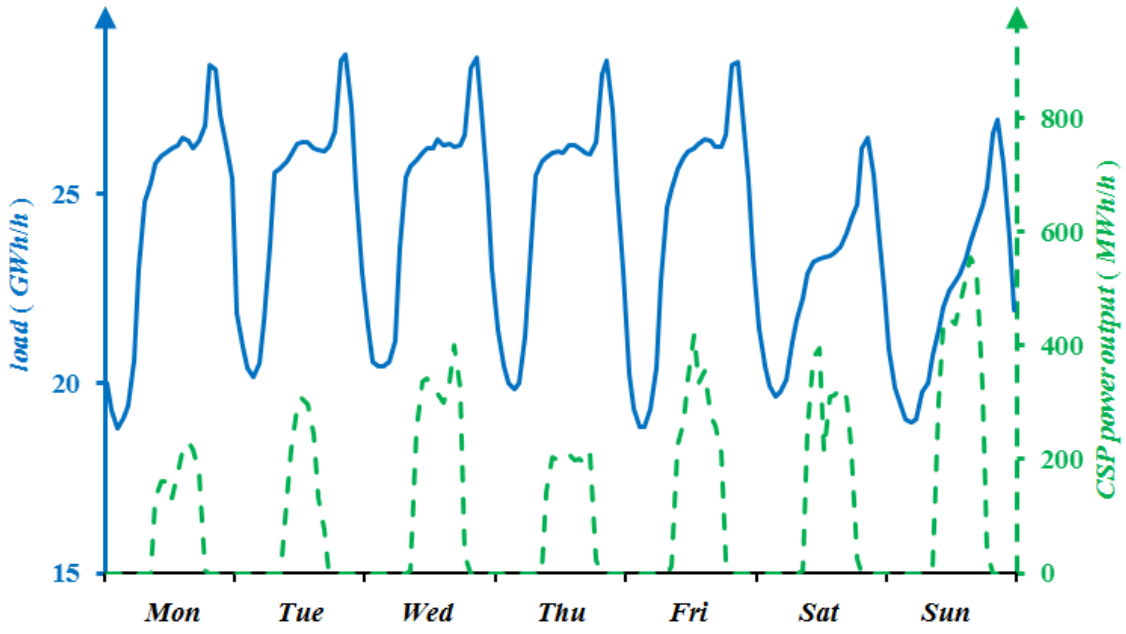

Figure 1.5: Plots of the chronological *CAISO* hourly loads and *CSP* power outputs for the March 10–16, 2014 [9]

1.2. Survey of the State of the Art

The integration of the *CSP* resources into the electric grid has become increasingly important in recent years with deepening *CSP* resource penetration. Here, we briefly review the literature related to the issues we are dealing with in this thesis.

The modeling of the *DNI* and the *CSP* are the two key issues that need to be addressed in the studies of systems with integrated *CSP* resources. The models' complexity depends on the nature of the study and the level of detail of the phenomena we want to capture. Due to the time dependence of the earth's and sun's movements, the temporal effects are always taken into account in the *DNI* modeling. For instance, the actual *DNI* value is computed based on the clear-sky *DNI* value, which is determined by the time of the year, and the atmospheric attenuation factor, which is approximated as a nonlinear function of the geographical information [10]. For systems with dispersed *CSP* resources over a broad area, the geographical correlations among the *DNI* also needs to be considered. In the solar irradiation forecasting area, some computationally demanding methods are reported in [11], [12] for *PV* resources. But those methods are only useful for short-term operational decision and are inappropriate for longer-term planning.

Researchers have developed multiple models to emulate the behaviors of *CSP* resources. Many of those techniques, described in [13], [14], [15], [16], focus on energy analysis and consider only the energy production from the *CSP* resources without the evaluation of their impacts on the system into which they are integrated. Although the methods in [17] probabilistically represent the load, the controllable resources and the renewable energy resources and the interplay among the resources and loads, the utilization of Monte Carlo methods is computationally demanding to simulate larger power systems, and

modifications are required to simulate the operations of the systems with integrated *CSP* resources. Several comprehensive studies have also studied the impacts of the wind and *PV* resource integration for several U.S. systems [18], based on chronological production simulations where the system operations are simulated step by step.

As a result, the electric power industry recognizes the need for new methods to effectively assess the impacts of uncontrollable renewable energy sources [19] and is intensified by the deepening renewable energy penetration.

1.3. Scope and Contributions of the Thesis

Little work has been done to construct a probabilistic simulation approach to emulate the realistic power system operations with integrated multi-site *CSP* resources, particularly over longer-term periods. The major challenge is to incorporate the additional uncertain and time-varying effects of *CSP*s into the approach [20], [21]. Such an approach needs to take into account the seasonality of loads and *CSP* resources, in addition to the *TES* operation scheduling and its impacts on *CSP* outputs. It also needs to explicitly represent interactions among loads and conventional controllable units. We address those needs to develop such an approach in this thesis.

We extend the conventional probabilistic simulation tool to construct a practical and versatile approach to effectively assess, over longer-term periods, the variable effects of systems with integrated *CSP*s at different sites. We develop a multi-site *CSP* power output model and formulate a *TES* scheduling problem (*SP*) to determine the daily multi-site *CSP* power outputs using the given daily *DNI* values. For the effective use of the historical *DNI* measurements to simulate the *CSP* power outputs, we introduce a common time scale to

allow the meaningful comparison of daily multi-site *DNI* data in a specific season and deploy statistical clustering techniques to obtain an analytic characterization of the daily multi-site *DNI* to construct the *DNI* regimes. We use the *CSP* power output model and the regime-based *DNI* characterization to probabilistically represent the power outputs of *CSP*s at distinct sites. We apply conditional probability concepts to incorporate the probabilistic multi-site *CSP* power output representation into the extended probabilistic simulation framework.

As such, the proposed methodology explicitly represents the uncertainty, variability and intermittency of the *CSP* power outputs, the flexibility imparted by *TES*, as well as the interactions among loads and resources. It also captures the seasonality of the loads and *CSP* resources. The primary application of the extended approach is to evaluate the contribution of integrated *CSP* resources to the power system over longer-term periods. We illustrate the effectiveness of the proposed approach using representative results from the extensive studies we performed on systems in different geographic regions under a wide range of conditions. The studies we discuss provide a realistic assessment of the impacts of the multi-site *CSP* resource integration on the systems' reliability, economic and environmental metrics.

1.4. Outline of the Thesis Contents

This thesis consists of four additional chapters. In Chapter 2, we focus on the probabilistic characterization of the multi-site *CSP* resources for the simulation purposes. We start with the modeling of the development of a deterministic model of the multi-site *CSP* power output. Then, we focus on the *DNI* data processing for utilization to analytically

characterize the multi-site *CSP* resources. In Chapter 3, we briefly review the conventional probabilistic production simulation tool and describe the steps to extend the production simulation with integrated *CSP* resources. We describe the modified version of the WECC test system in Chapter 4 and select some representative results from the extensive studies we performed to illustrate the application of the extended probabilistic simulation approach. We conclude our contributions and provide directions for future work in Chapter 5. There are three appendixes at the end of the thesis. In Appendix A, we summarize the notations used in this thesis. We describe in detail the scaling and descaling algorithms in Appendix B and C, respectively.

2. THE PROBABILISTIC MULTI-SITE *CSP* RESOURCE POWER OUTPUT MODEL

The quantification of the variable impacts, over longer-term periods, of the multi-site *CSP* resources integrated into a power system requires the construction of a multi-site *CSP* power output model, which explicitly represents the uncertainty, intermittency and variability of the locational *DNI* and their impacts on the *CSP* outputs. We devote this chapter to the description of the proposed multi-site *CSP* generation model and its deployment to probabilistically characterize such outputs.

This chapter contains three sections. In Section 2.1, we derive a solution for an optimization problem to determine the multi-site *CSP* power outputs, using the given *DNI* values. In Section 2.2, we develop the probabilistic characterization of the locational *DNI*s and introduce the notion of multi-site *DNI regimes* to explicitly represent the salient *DNI* patterns in distinct geographical areas. We use the scaling algorithm to scale the historical *DNI* data onto a common time scale so as to identify the days with similar scaled *DNI* shapes. We introduce the descaling algorithm to convert the scaled *DNI* samples onto the actual sunrise-to-sunset period of the day for simulation purposes. In Section 2.3, we analytically characterize the multi-site *CSP* power outputs and describe the approximation of the regime-conditioned distribution functions of the *CSP* power output random variables (*r.v.*s). We use the notations defined in Appendix A.

2.1. The Deterministic Multi-site *CSP* Generation Model

We start this section with a brief description of the behavior of a stand-alone *CSP*. Many conventional and nuclear power plants use heat to boil water to produce high-pressure

steam, which expands through the turbine to spin the generator rotor to produce electricity. *CSP* technology extracts the heat from the solar energy and, in a way similar to the conventional or nuclear plants, produces steam to generate electricity. A typical *CSP* set-up includes four primary components: collectors that concentrate solar rays, receivers that collect and convert solar energy into thermal energy, the *TES* that stores thermal energy for later use, and a power block that converts thermal energy into electricity. We refer to the collection of collectors and receivers as the solar field. We summarize in Fig. 2.1 the energy flows in a typical *CSP*.

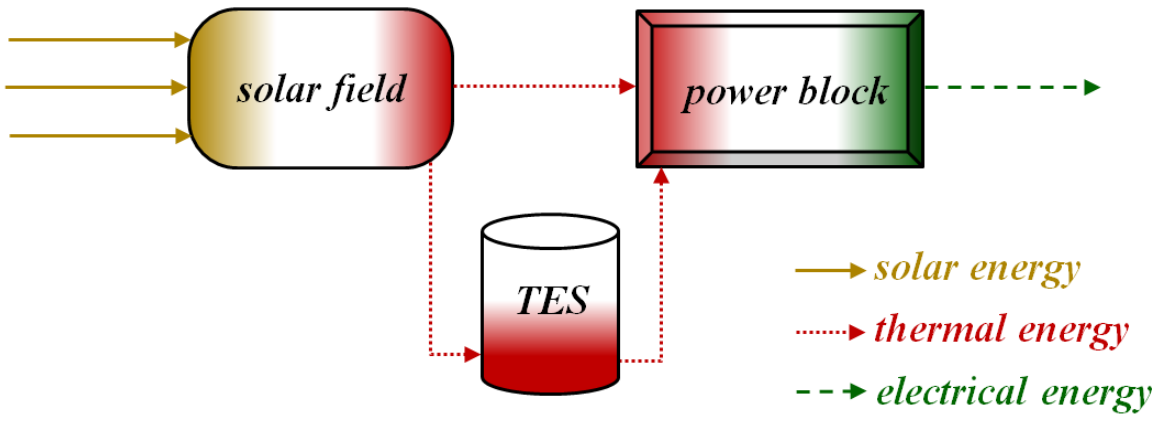

Figure 2.1: Energy flows in a typical *CSP*

For a power system with integrated *CSP*s at multiple locations, the power output of each *CSP* depends on the *DNI* at its location, the specific *CSP* configuration and the utilization schedule of the *TES*. The aggregated power produced by the *CSP*s must take into account the correlations among the *DNI*s at the multiple locations. The *CSP* converts the solar energy into thermal energy, used instantaneously either to generate electricity in the turbines or to be stored in the *TES* for later conversion. The utilization of the *TES* allows

the *CSP* to produce electricity even outside the sunrise-to-sunset periods and to smooth the total output of the *CSP* units. Moreover, the *TES* deployment enables the *CSP* operator to construct a multi-site *TES* schedule to meet some specific operational objective, such as the maximization of the total energy produced by the multi-site *CSP*s or the provision of a smoothed, aggregated multi-site *CSP* power output. Such *TES* schedules lead to the inter-temporal and spatial coupling of *CSP* operations at the different locations. We note that the thermal energy can be charged into/discharged from the *TES* without the violation of each *TES'*s maximum/minimum capability. The *TES* physical capability refers to the maximum amount of thermal energy that can be stored in the *TES*. The storage hour capability is expressed as the ratio of the physical capability to the maximum input of power block for electricity generation [22]. The charging/discharging rate of each *TES* device must be within its capacity range and the *TES* device operates at any point in time in only one of its operational states – charge, discharge or idle. A *TES* device cannot charge and discharge simultaneously. Typically, due to the nature of *TES*, the thermal energy also incurs losses over time [23]. Such losses are specified either in terms of *%* or as a loss rate of energy in units of $\mathrm{MWh_t/h}$.

We construct the power output model of a system with integrated *CSP*s at *S* sites to emulate the multi-site *CSP* operations with *TES* for each day in a simulation period. For simplicity, we assume that there is a single *CSP* at each site *s*. In the case of multiple *CSP*s at a site *s*, we construct an equivalent single *CSP* to represent the aggregated individual *CSP* outputs at the site. We decompose each day into *H* equal-duration sub-periods. We assume that each variable of interest, except the value of stored energy, remains constant during a sub-period. Since the energy storage is of critical interest, we adopt the

convention that we represent the value of each variable, including thermal energy stored, at the end of each sub-period. The system loads and the *DNI* values for each sub-period are assumed given. A sub-period is the smallest, indecomposable unit of time and determines the resolution of the simulation. Any phenomenon of shorter duration than a sub-period cannot be represented and so is ignored.

The instantaneous solar-to-thermal energy conversion at site *s* is given by the nonlinear mapping $\beta_s(\cdot)$, whose argument is the *DNI* $u_s^d[h]$. Since the plant design of *CSP* is out of the scope of the thesis, $\beta_s(\cdot)$ is not explicitly formulated in this work. We rely on the *Solar Advisor Model* [22] – a dynamic model developed by *NREL* – to determine the amount of thermal energy collected by the solar field in each sub-period for the geographic, weather and time input data of the *CSP*s. The nonlinear mapping $\alpha_s(\cdot)$, whose argument is the thermal energy $z_s^d[h]$, is used to instantaneously convert the thermal energy into electricity:

$$\alpha_s\left(z_s^d[h]\right) = c_s\left(\Lambda_{s,4}\left(\frac{z_s^d[h]}{z_s^{max}}\right)^4 + \Lambda_{s,3}\left(\frac{z_s^d[h]}{z_s^{max}}\right)^3 + \Lambda_{s,2}\left(\frac{z_s^d[h]}{z_s^{max}}\right)^2 + \Lambda_{s,1}\left(\frac{z_s^d[h]}{z_s^{max}}\right)^1 + \Lambda_{s,0}\right) \quad (2.1)$$

Here c_s represents the site *s CSP* capacity, z_s^{max} represents the thermal energy input rate needed to guarantee that the site *s* power block produces electricity at its rated capacity and $\Lambda_{s,i}$ are function coefficients, *i* = 0, 1, …, 4 [22]. We utilize the *TES* status variables $v_s^d[h]$, $\varphi_s^d[h] \in \{0,1\}$ to define the operational state of a *TES* device. $v_s^d[h]$ ($\varphi_s^d[h]$) is equal to 1 when the *TES* charges (discharges). Both are 0 when the *TES* device is idle. $\varepsilon_s^d[h]$ denotes the stored thermal energy at the end of the sub-period *h.* We represent the *TES* charging

(discharging) efficiency by the constant η_s (μ_s) $\in (0,1]$. We also denote the thermal energy loss rate, expressed in units of percent per sub-period, by the constant ψ_s. The *TES* physical and operational capability limits are given by ε_s^{min} and ε_s^{max*}. The sub-period charging (discharging) rate $k_s^d[h]$ ($q_s^d[h]$) has values within its allowed $\left[k_s^{min}, k_s^{max}\right]$ ($\left[q_s^{min}, q_s^{max}\right]$) range.

We formulate the *scheduling problem* (*SP*) [13], [14], [22], [23], [24], [25], to determine the optimal day *d* operational trajectory of each *CSP* with *TES*, using the hourly *DNI* values in the array $\left[\underline{\boldsymbol{u}}_1^d \vdots \underline{\boldsymbol{u}}_2^d \vdots \ldots \vdots \underline{\boldsymbol{u}}_S^d\right]$. The *SP* is formulated as a constrained optimization problem. The set of constraints comes from the *TES* physical characteristics and operational limits. For the specified *TES* objective function, each coefficient $\gamma_s^d[h]$ can be determined either from historical data or from forecasts or be some given values. The detailed statement of the daily *SP* for day *d* is:

$$\max_{\substack{\{k_s^d[h], v_s^d[h], q_s^d[h], \varphi_s^d[h], \varepsilon_s^d[h], \\ z_s^d[h], p_s^d[h], h=1,2,...,H, s=1,2,...S\}}} \sum_{h=1}^{H}\sum_{s=1}^{S} \gamma_s^d[h]\ p_s^d[h]\ \Delta \qquad (2.2a)$$

subject to

* The *physical capability* ε_s^{max}, expressed in the units of MWh_t, refers to the maximum amount of stored thermal energy; the storage capability is expressed as the ratio of the physical capability to maximum input of power block for electricity generation. The *TES* capability, expressed in hour units, is the ratio of ε_s^{max} to z_s^{max}.

$$
\left.
\begin{aligned}
& \varepsilon_s^d[h] \le (1-\psi_s)\varepsilon_s^d[h-1] + \eta_s k_s^d[h]\Delta - q_s^d[h]\Delta_H && (2.2b)\\
& v_s^d[h] + \varphi_s^d[h] \le 1 && (2.2c)\\
& z_s^d[h] \le \beta_s\left(u_s^d[h]\right) - k_s^d[h] + \mu_s q_s^d[h] && (2.2d)\\
& p_s^d[h] = \alpha_s\left(z_s^d[h]\right) && (2.2e)\\
& \varepsilon_s^{min} \le \varepsilon_s^d[h] \le \varepsilon_s^{max} && (2.2f)\\
& z_s^{min} \le z_s^d[h] \le z_s^{max} && (2.2g)\\
& v_s^d[h]\, k_s^{min} \le k_s^d[h] \le v_s^d[h]\, k_s^{max} && (2.2h)\\
& \varphi_s^d[h]\, q_s^{min} \le q_s^d[h] \le \varphi_s^d[h]\, q_s^{max} && (2.2i)\\
& v_s^d[h], \varphi_s^d[h] \in \{0,1\} && (2.2j)
\end{aligned}
\right\}
\quad h = 1, 2, \ldots, H; \quad s = 1, 2, \ldots, S
$$

For the given *DNI* values, the solution of the deterministic *SP* in (2.2) determines the optimal multi-site *CSP* operations and power outputs for each sub-period of day *d*. Without *TES*, no scheduler is needed since all the thermal energy is instantaneously converted to electricity with

$$p_s^d[h] = \alpha_s\left(\beta_s\left(u_s^d[h]\right)\right) \tag{2.3}$$

To illustrate the application of *SP* in our work, we provide in Figure 2.2 the plots of the hourly power outputs for day 180 of year 2007 of a *CSP* located at Midland, Texas, without/with a *TES* device. The *CSP* parameters are: $\eta_s = \mu_s = 0.95$, $\psi_s = 0.03$, $\varepsilon_s^{min} = 0$, $\varepsilon_s^{max} = 0$ *or* 840 $\mathrm{MWh_t}$, $z_s^{min} = 50\ \mathrm{MW_t}$, $z_s^{max} = 140\ \mathrm{MW_t}$, $\left[k_s^{min}, k_s^{max}\right] = \left[q_s^{min}, q_s^{max}\right] = [0, 140]\ \mathrm{MW_t}$, $c_s = 60\mathrm{MW}$ and $\left[\Lambda_{s,4}, \Lambda_{s,3}, \Lambda_{s,2}, \Lambda_{s,1}, \Lambda_{s,0}\right] = [0, 0, 0, 0, 0.3]$. Each

objective function coefficient is set to 1.

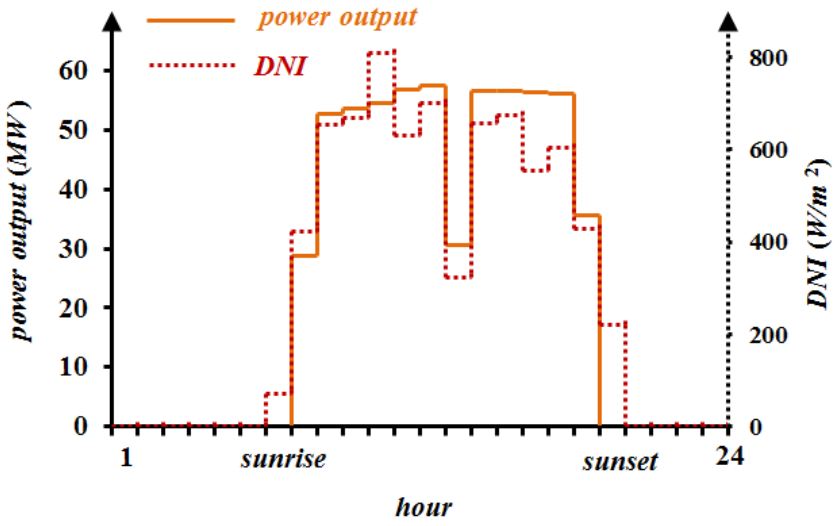

(*a*) without *TES*

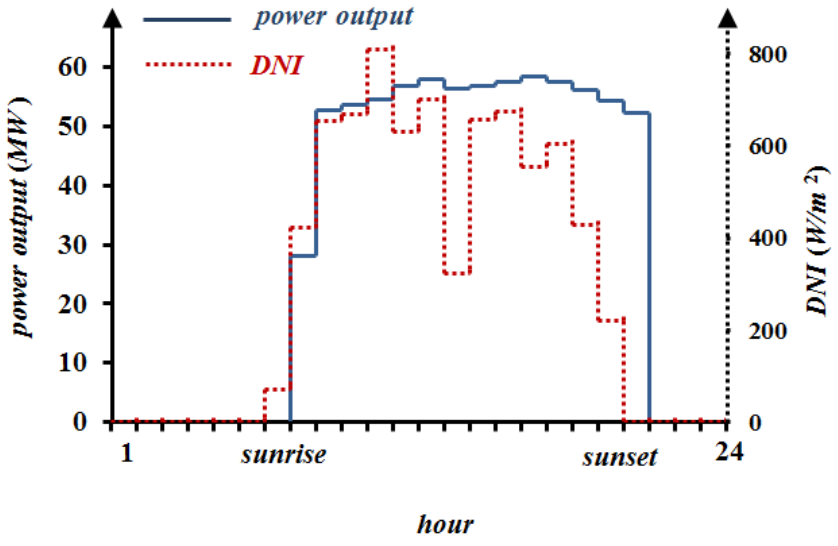

(*b*) with 6-hour *TES*

Figure 2.2: The *CSP* power outputs without *TES* in (*a*) and with 6-hour *TES* in (*b*) for day 180 *DNI* (dotted line) in year 2007 at Midland, Texas

As shown in Fig.2.2 (*a*), the *CSP* energy production at each hour without *TES* is totally determined by its hourly *DNI* value. When the *DNI* value is low, the *CSP* power output is low, and when the *DNI* value is high, the *CSP* power output is high but cannot violate its capacity. In Fig.2.2 (*b*), the *TES* stores thermal energy for electricity production and mitigates the impacts of *DNI* intermittency on the *CSP* energy production. The two plots in this example illustrated the capability of *SP* formulation to emulate the behavior of *CSP* resource without and with *TES*.

The *SP* forms the basis to characterize the multi-site *CSP* power outputs. However, for each day *d*, the locational *DNI* values are highly uncertain and so we represent them as the realizations of the *DNI* random variables (*r.v.*s) at the *S* sites. The historical data $\left[\underline{\boldsymbol{u}}_1^d \vdots \underline{\boldsymbol{u}}_2^d \vdots \ldots \vdots \underline{\boldsymbol{u}}_S^d\right]$ are indeed the measured values of these *r.v.*s. As such, the *SP* solution maps these *DNI* realizations into the realizations of the power output *r.v.*s. $\left[\underline{\boldsymbol{p}}_1^d \vdots \underline{\boldsymbol{p}}_2^d \vdots \ldots \vdots \underline{\boldsymbol{p}}_S^d\right]$. In this way, we probabilistically characterize the multi-site *CSP* power outputs.

2.2. The Multi-site *DNI* Model

As the first step in the probabilistic characterization of the *CSP* power outputs, we analyze the multi-site *DNI* data obtained from the measurements at the *S* sites. A single measurement is used in each sub-period at each site. We assume that these measurements are made simultaneously at all the *S* sites in each sub-period during each site's sunrise-to-sunset period. For a probabilistic characterization, we use as many data points as we can collect. However, the analysis of these data is complicated by the variations in the sunrise-

to-sunset periods at the *S* sites. We consider a data set of *I* days in a given season, with possibly several years of data collected. The date of each day *i* in the data collection is known, as are the corresponding sunrise and sunset times at each site *s*. From the M_s^i *DNI* measurements $\hat{u}_s^i[m]$ taken at equal intervals during the sunrise-to-sunset period in day *i*, we construct the corresponding *DNI* measurement vector :

$$\underline{\hat{\boldsymbol{u}}}_s^i = \begin{bmatrix} \hat{u}_s^i[1] \\ \vdots \\ \hat{u}_s^i[m] \\ \vdots \\ \hat{u}_s^i\left[M_s^i\right] \end{bmatrix} \in \mathbb{R}^{M_s^i} \tag{2.4}$$

To allow the effective comparisons of the *DNI* data from different days of a season, we introduce a scaling scheme over the sunrise-to-sunset period of each day into the common time scale with *J* equal-duration time-scaled sub-periods. The scaling process maps the measurement elements in $\underline{\hat{\boldsymbol{u}}}_s^i$ into the computed vector $\underline{\boldsymbol{y}}_s^i \in \mathbb{R}^J$ on the common time scale. Mathematically, we represent the scaling process as the transformation from $\mathbb{R}^{M_s^i}$ into $\mathbb{R}^J$ and express it as:

$$\underline{\boldsymbol{y}}_s^i = \underline{\boldsymbol{\theta}}_s^i(\underline{\hat{\boldsymbol{u}}}_s^i) = \begin{bmatrix} y_s^i[1] \\ \vdots \\ y_s^i[j] \\ \vdots \\ y_s^i[J] \end{bmatrix} \in \mathbb{R}^J \tag{2.5}$$

We visualize the time scaling process as shown in Fig. 2.3.

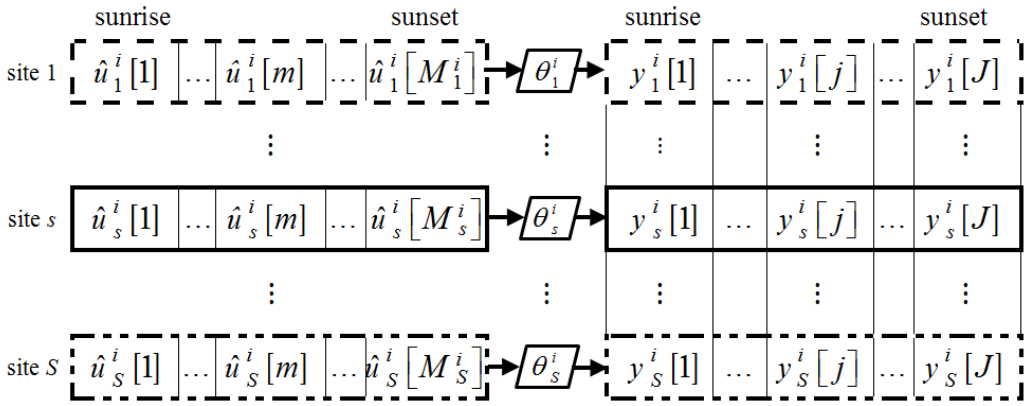

Figure 2.3: The time scaling process in day *i* at the *S* sites produces the computed *DNI* values for *J* equal time-scaled sub-periods from sunrise to sunset

We provide in Fig. 2.4 an illustrative example of the application of this scaling process to the single Las Vegas, Texas, *DNI* shapes for year 2013. The detailed steps of scaling algorithm are discussed in Appendix B in [26].

We continue with the discussion on the use of the common-time-scaled computed variables $\underline{\boldsymbol{y}}_s^i$. For each day *i*, we construct the scaled *DNI* array

$$\underline{\bar{\boldsymbol{Y}}}^i = \left[\underline{\boldsymbol{y}}_1^i \vdots\ \underline{\boldsymbol{y}}_2^i \vdots\ \ldots \vdots\ \underline{\boldsymbol{y}}_S^i\right] \in \mathbb{R}^{J\times S} \tag{2.6}$$

using the *S* vectors $\underline{\boldsymbol{y}}_s^i$, *s* = 1, 2, …, *S*. $\underline{\bar{\boldsymbol{Y}}}^i$ represents realizations of the daily multi-site *DNI* on the common time scale at the *S* sites. As shown in Figure 2.5, we collect arrays $\underline{\bar{\boldsymbol{Y}}}^i$ for *I* days and construct the set

$$\mathcal{Y} = \{\underline{\bar{\boldsymbol{Y}}}^i : i = 1, 2, \ldots, I\} \tag{2.7}$$

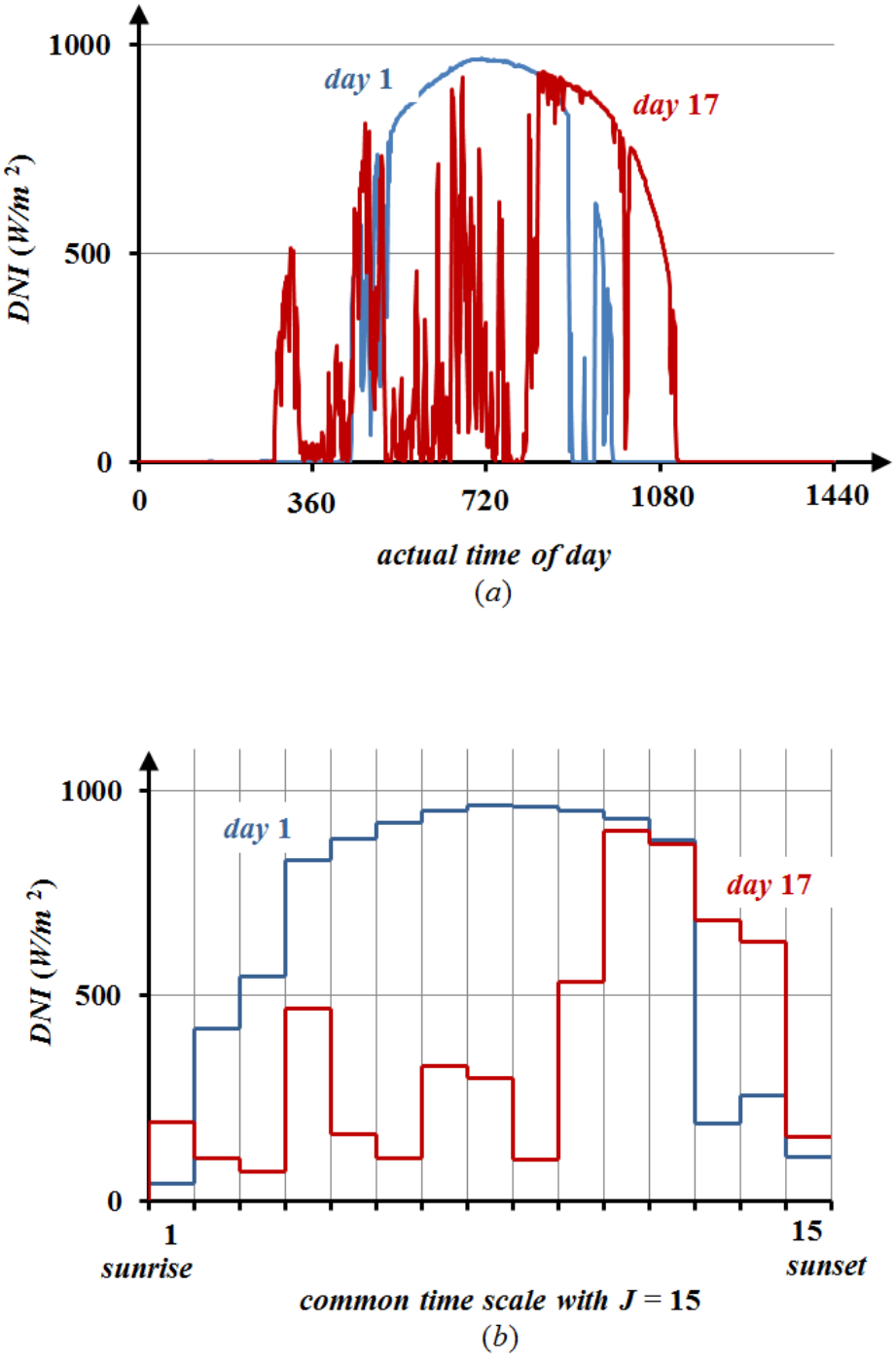

Figure 2.4: The measured and the common time scale with J = 15 winter season hourly *DNI* values in (*a*) and (*b*), respectively, for two different days in year 2013 winter season at a Las Vegas, Texas location [7]

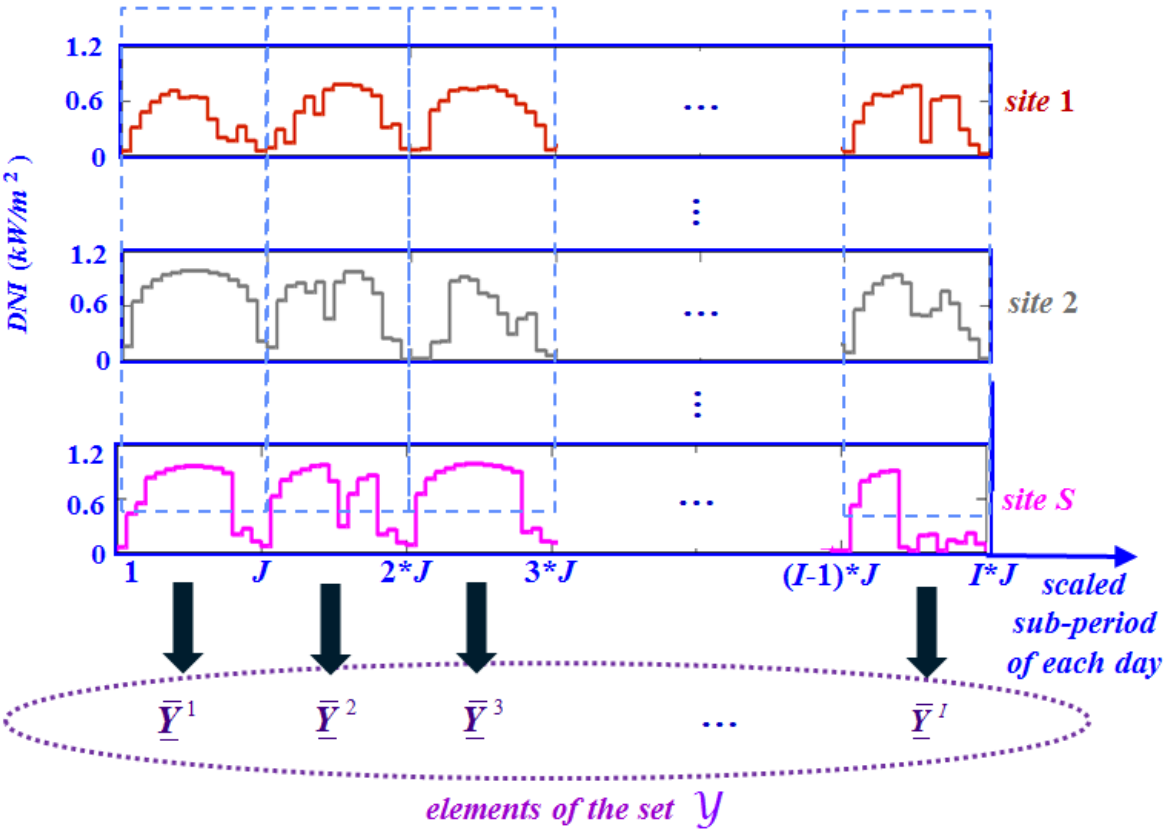

Figure 2.5: Collection of seasonal daily scaled *DNI* shapes at *CSP* sites

We view the set $\mathcal{Y}$ to be the sample space of the *S*-site *DNI r.v.*s on the common time scale. The set $\mathcal{Y}$ provides the basis for the identification of *similar* daily *DNI* realizations via the deployment of statistical clustering techniques. In this way, we classify the samples in the set $\mathcal{Y}$ into *R* non-overlapping clusters $\mathcal{R}_r$, $r = 1, 2, \ldots, R$, as shown in Fig. 2.6. Each cluster groups together a subset of *similar* time-scaled daily multi-site *DNI* realizations:

$$\mathcal{R}_r \bigcap \mathcal{R}_{r'} = \varnothing, \; r \neq r' \tag{2.8}$$

$$\mathcal{Y} = \bigcup_{r=1}^{R} \mathcal{R}_r \tag{2.9}$$

The cardinality $|\mathcal{R}_r|$ of each cluster $\mathcal{R}_r$, $r = 1, 2, \ldots, R$, provides the basis to compute the cluster probability in terms of the fraction of the I days that belong to the cluster, *i.e.*,

$$\pi_r = \frac{|\mathcal{R}_r|}{I} \tag{2.10}$$

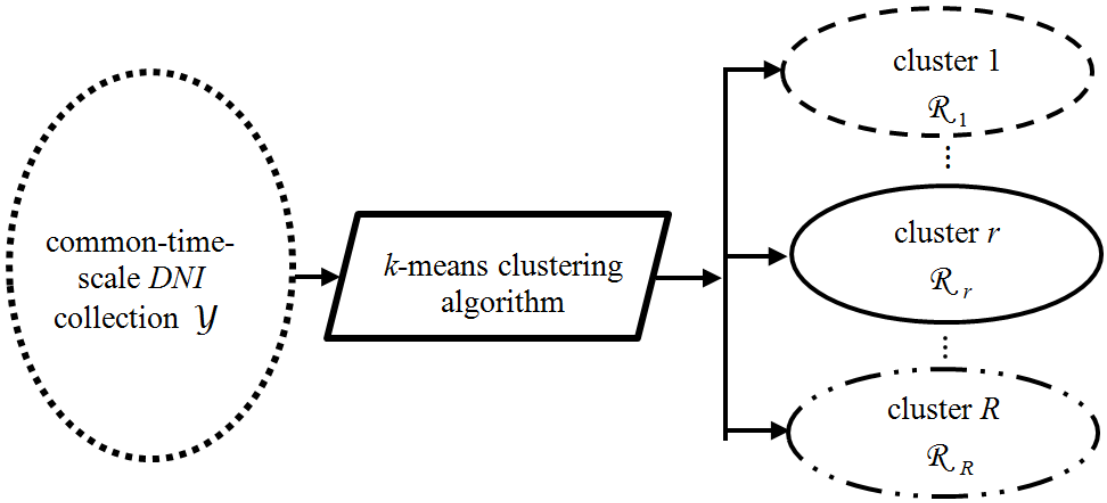

Figure 2.6: Diagram representation of the clustering process

We refer to the cluster $\mathcal{R}_r$ and its probability π_r as the regime $\mathscr{R}_r$. We represent each $\mathscr{R}_r$ by the $\mathcal{R}_r$ centroid, to which we refer as the regime r daily *DNI pattern*.

For an example of actual data, we scale and classify 2005 summer *DNI* data at Abilene, Lubbock and Midland in Texas, into four regimes, whose centroids are plotted in Fig. 2.7.

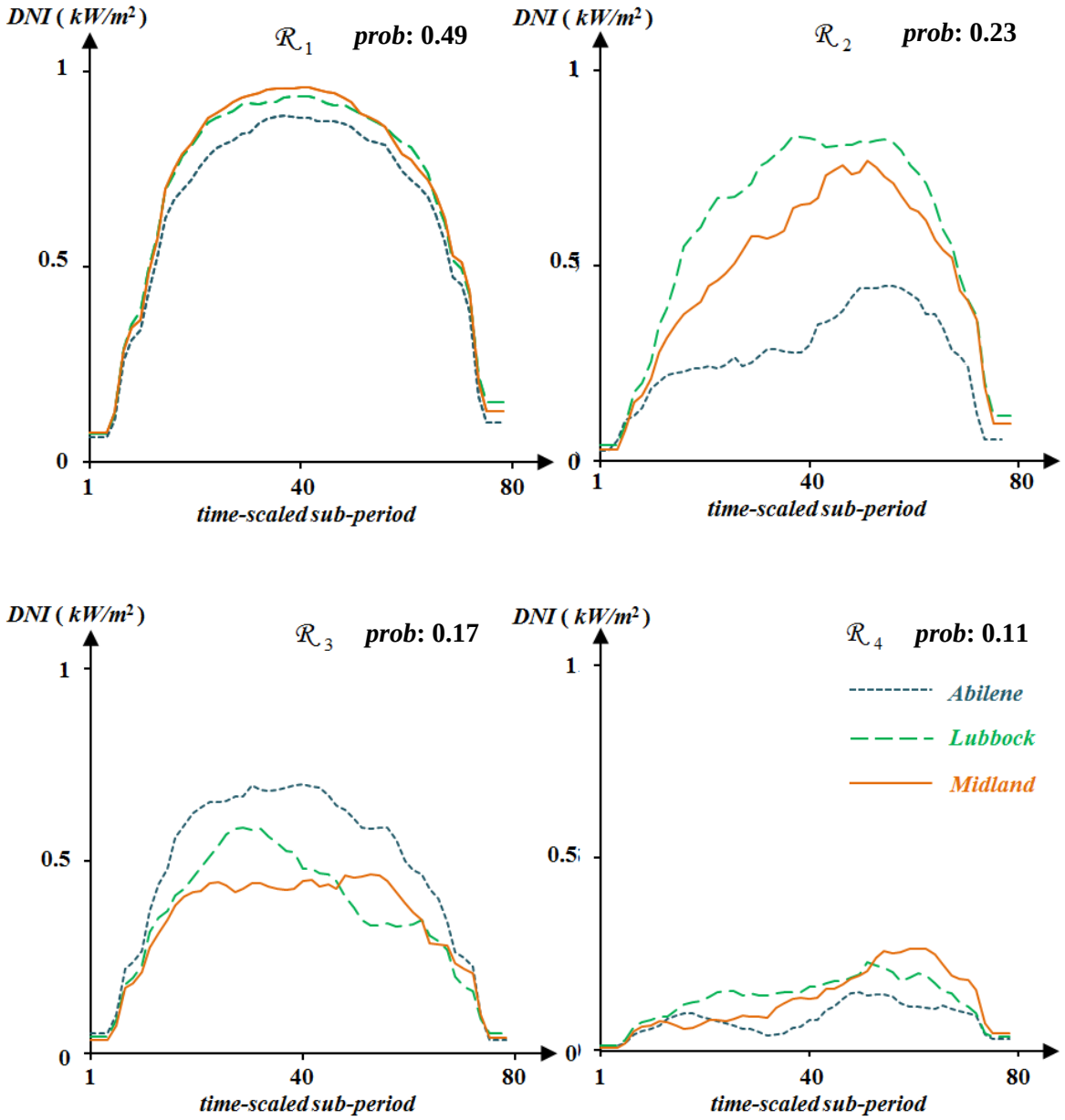

Figure 2.7: The centroids of the common-time-scale computed values of the four *DNI* regimes with $J = 80$, obtained via the k-means clustering algorithm [27], for the summer *DNI* data at the three Texas sites – Abilene, Lubbock and Midland

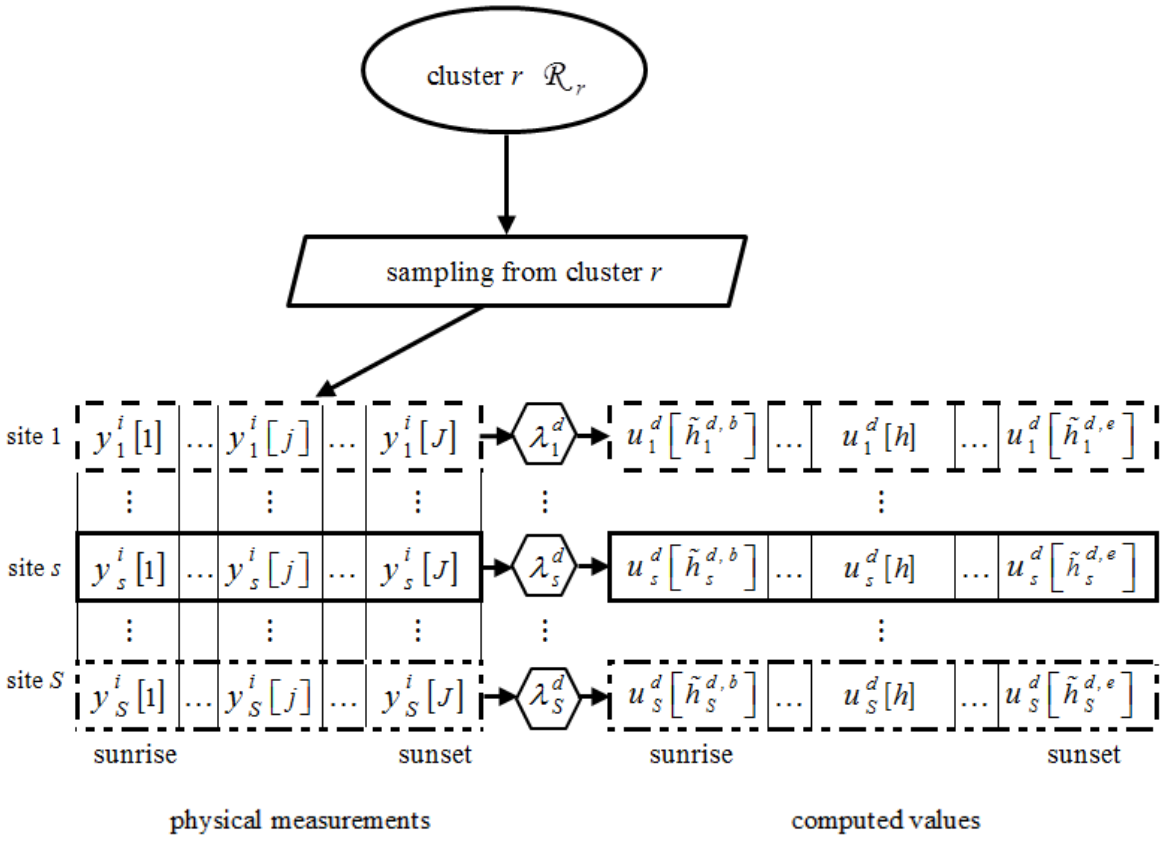

Figure 2.8: The representation of the sampling of the physical measurements and the descaling process for the computation of the day *d* data at the *S CSP* sites

We make effective use of conditional probability to probabilistically characterize the multi-site *CSP* resources in terms of the *R* regime representation [28]. We draw random samples from each cluster $\mathcal{R}_r$ to use as inputs into the multi-site *CSP* power output model. The simulation of a specified day *d* in the given season requires that a sample be appropriately descaled into the day *d* multi-site sunrise-to-sunset periods. We descale the *J* *DNI* values at each site *s* in the drawn common time scale sample into the computed *DNI* values $\left[u_s^d\left[\tilde{h}_s^{d,b}\right], u_s^d\left[\tilde{h}_s^{d,b}+1\right], \ldots, u_s^d\left[\tilde{h}_s^{d,e}\right]\right]^T$ for the $(\tilde{h}_s^{d,e}-\tilde{h}_s^{d,b}+1)$ equal-duration sub-periods in the day *d* sunrise-to-sunset period at each site *s*. We represent the descaling

process by the transformation λ_s^d. We summarize in Fig. 2.8 the sampling and descaling step.

To maintain consistency of the midnight-to-midnight representation of the loads, we use the components of the descaled vector $\left[u_s^d\left[\tilde{h}_s^{d,b}\right], u_s^d\left[\tilde{h}_s^{d,b}+1\right], \ldots, u_s^d\left[\tilde{h}_s^{d,e}\right]\right]^T$ to construct the augmented daily vector for the entire *H*-sub-period day with

$$\underline{\boldsymbol{u}}_s^d = \begin{bmatrix} u_s^d[1] \\ \vdots \\ u_s^d\left[\tilde{h}_s^{d,b}\right] \\ \vdots \\ u_s^d\left[\tilde{h}_s^{d,e}\right] \\ \vdots \\ u_s^d[H] \end{bmatrix} \in \mathbb{R}^H \tag{2.11}$$

where $\underline{\boldsymbol{u}}_s^d$ represents the day *d* site *s DNI* realizations from midnight to midnight, with:

$$u_s^d[h] = 0 \text{ for } h \in [1, \tilde{h}_s^{d,b} - 1] \bigcup [\tilde{h}_s^{d,e} + 1, H] \tag{2.12}$$

To illustrate the descaling and the augmented vector construction, we provide in Figure 2.9 the plots of the common time scale *DNI* data and the daily descaled *DNI* for day 165 of year 2013 at Austin, Texas. The vector $\underline{\boldsymbol{u}}_s^d$ is simply a realization of the *r.v.* vector:

$$\underline{\boldsymbol{U}}_s^d = \begin{bmatrix} \underset{\sim}{U}_s^d[1] \\ \vdots \\ \underset{\sim}{U}_s^d[h] \\ \vdots \\ \underset{\sim}{U}_s^d[H] \end{bmatrix} \in \mathbb{R}^H \tag{2.13}$$

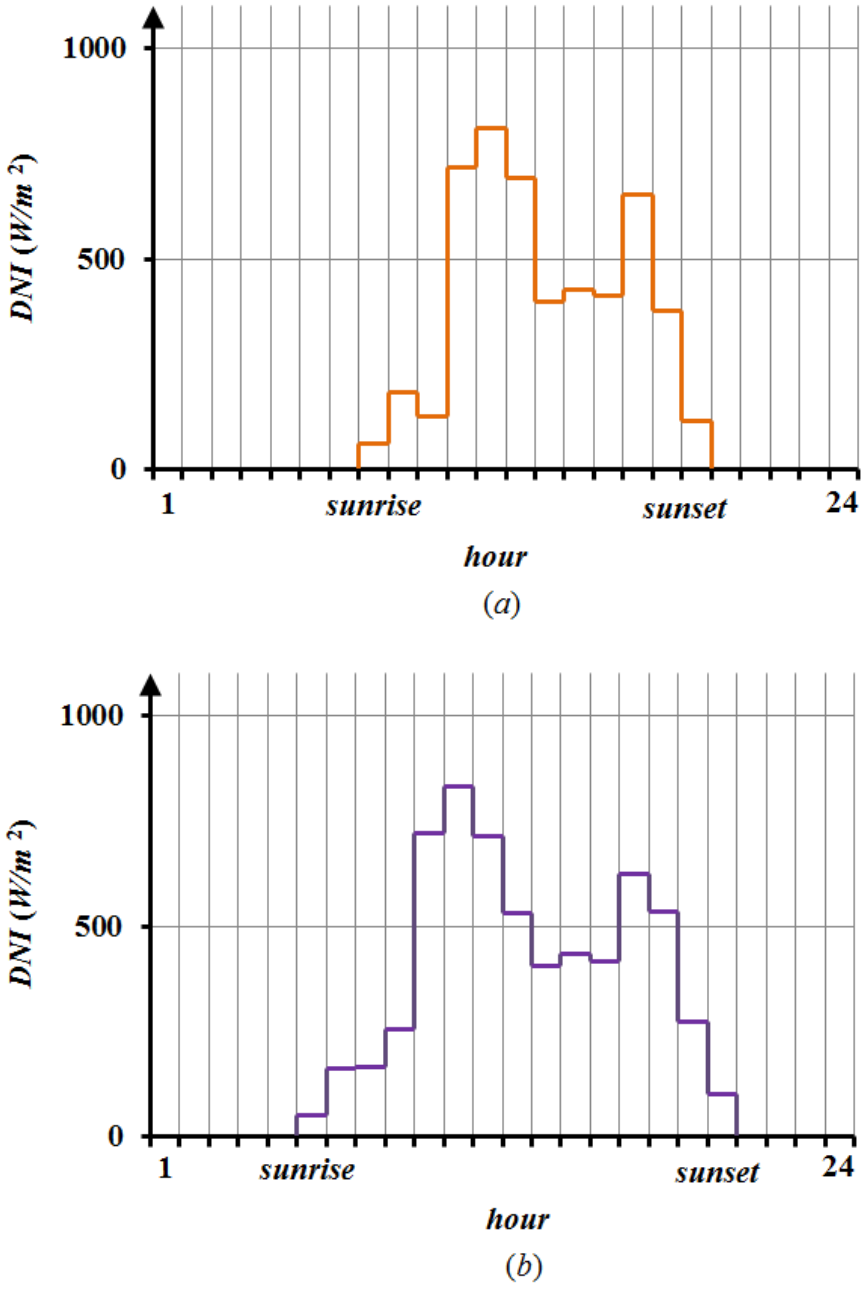

Figure 2.9: The common time scale with $J = 20$ values of a sample we used to construct the *DNI* vector for day 165 of year 2013 at Austin, Texas in (*a*) with the corresponding values of the daily descaled *DNI* vector ($H = 24$) in (*b*) [7]

We denote the realization of the *r.v.* vector $\underset{\sim}{\boldsymbol{U}}_s^d$ conditioned on the cluster $\mathcal{R}_r$, *i.e.*, $\underset{\sim}{\boldsymbol{U}}_s^d\Big|_r$, by the augmented vector $\underline{\boldsymbol{u}}_s^d\Big|_r$. We construct the *DNI r.v.* array $\bar{\underset{\sim}{\boldsymbol{U}}}^d$ from the *S* vectors:

$$\bar{\underset{\sim}{\boldsymbol{U}}}^d = \left[\underset{\sim}{\boldsymbol{U}}_1^d \vdots \underset{\sim}{\boldsymbol{U}}_2^d \vdots \ldots \vdots \underset{\sim}{\boldsymbol{U}}_S^d\right] \in \mathbb{R}^{H\times S} \tag{2.14}$$

and the corresponding *DNI r.v* array conditioned on cluster $\mathcal{R}_r$:

$$\bar{\underset{\sim}{\boldsymbol{U}}}^d\Big|_r = \left[\underset{\sim}{\boldsymbol{U}}_1^d\Big|_r \vdots \underset{\sim}{\boldsymbol{U}}_2^d\Big|_r \vdots \ldots \vdots \underset{\sim}{\boldsymbol{U}}_S^d\Big|_r\right] \in \mathbb{R}^{H\times S} \tag{2.15}$$

For given *DNI* values, the solution of the *SP* that maximizes the objective function in (2.2*a*) in (2.2) is the optimal multi-site *CSP* power outputs at the *S* sites. In particular, for a given sample of conditioned multi-site *DNI r.v.*s – $\underset{\sim}{\boldsymbol{U}}_1^d\Big|_r$, $\underset{\sim}{\boldsymbol{U}}_2^d\Big|_r$, …, $\underset{\sim}{\boldsymbol{U}}_S^d\Big|_r$, the solution obtained the corresponding optimal sample of conditioned multi-site *CSP* power output *r.v.*s – $\underset{\sim}{\boldsymbol{P}}_1^d\Big|_r$, $\underset{\sim}{\boldsymbol{P}}_2^d\Big|_r$, …, $\underset{\sim}{\boldsymbol{P}}_S^d\Big|_r$, which are conditioned on cluster $\mathcal{R}_r$. We depict the mapping process in Figure 2.10 to indicate that the deterministic *SP* solution maps each sample into the conditioned optimal outputs. In this way, we obtain the multi-site *CSP* power output *r.v.* sample space, which we can deploy to approximate the multi-site *CSP* resource power output *r.v.*s cumulative distribution function (*c.d.f.*).

Thus, the *SP* together with multi-site *DNI* clusters provides the probabilistic characterization the multi-site *CSP* resource power output *r.v.*s . We devote the next section to the probabilistic characterizations of the *CSP* power outputs based on *SP* and the multi-site *DNI* model.

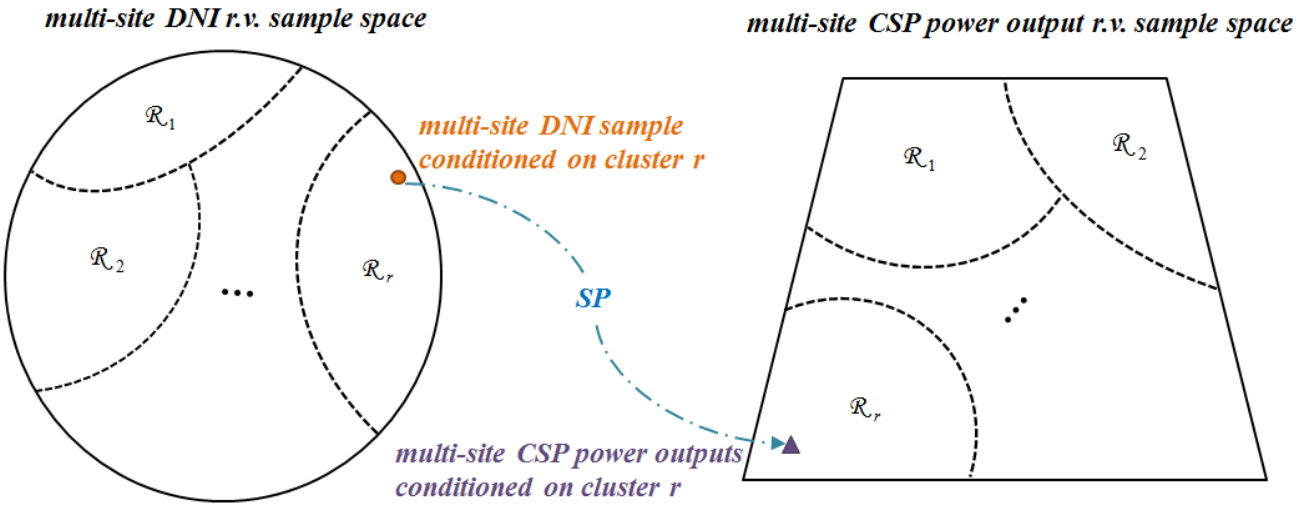

Figure 2.10: Mapping from the multi-site *DNI r.v.* sample space into the multi-site *CSP* power output *r.v.* sample space using the *SP*

2.3. The Probabilistic Characterization of the *CSP* Power Outputs

The regime-based *DNI* model provides the basis to construct the probabilistic model of the *CSP* power outputs. The *SP* solution for each input *DNI* sample drawn from a cluster $\mathcal{R}_r$ determines the corresponding conditioned *CSP* power output realization. We represent such a conditioned realization by the array $\underline{\bar{\boldsymbol{P}}}^{d}\big|_{r}$:

$$\underline{\bar{\boldsymbol{P}}}^{d}\big|_{r} = \left[\underline{\boldsymbol{p}}_{1}^{d}\big|_{r} \vdots \underline{\boldsymbol{p}}_{2}^{d}\big|_{r} \vdots \ldots \vdots \underline{\boldsymbol{p}}_{S}^{d}\big|_{r} \right] \in \mathbb{R}^{H \times S} \tag{2.16}$$

Mathematically, $\underline{\bar{\boldsymbol{P}}}^{d}\big|_{r}$ is the corresponding realization of the multi-site *CSP* power output *r.v.* array $\underset{\sim}{\underline{\bar{\boldsymbol{P}}}}^{d}$ conditioned on cluster $\mathcal{R}_r$, where:

$$\underset{\sim}{\bar{\boldsymbol{P}}}^{d}\Big|_{r} = \left[\underset{\sim}{\boldsymbol{P}}_{1}^{d}\Big|_{r} \vdots \underset{\sim}{\boldsymbol{P}}_{2}^{d}\Big|_{r} \vdots \ldots \vdots \underset{\sim}{\boldsymbol{P}}_{S}^{d}\Big|_{r} \right] \in \mathbb{R}^{H \times S} \tag{2.17}$$

The computation of the day *d* multi-site *CSP* power output requires that we sample from each cluster $\mathcal{R}_r$, r = 1, 2, …, R, and determine the corresponding conditioned realization of $\underset{\sim}{\bar{\boldsymbol{P}}}^{d}\Big|_{r}$. We use the conditioned realization of the power output for each sample drawn from a cluster $\mathcal{R}_r$ to construct the subspace of the sample space of $\underset{\sim}{\bar{\boldsymbol{P}}}^{d}$, with multiple samples from that particular cluster $\mathcal{R}_r$. We systematically repeat such a procedure for each regime $\mathscr{R}_r$ and obtain the R subspaces for each conditioned $\underset{\sim}{\bar{\boldsymbol{P}}}^{d}\Big|_{r}$, r = 1, 2, …, R. The sample space of $\underset{\sim}{\bar{\boldsymbol{P}}}^{d}$ is simply the union of the non-overlapping subspaces that we construct for the repeated sampling from the R clusters.

We compute the total aggregated conditioned power outputs of the *CSP*s at the S sites for each sub-period h to be:

$$p_{\Sigma}^{d}\Big|_{h,r} = p_{\Sigma}^{d}[h]\Big|_{r} = \sum_{s=1}^{S} p_{s}^{d}[h]\Big|_{r} \tag{2.18}$$

We then construct the daily power output vectors:

$$\underset{\sim}{\boldsymbol{p}}_{\Sigma}^{d}\Big|_{r} = \sum_{s=1}^{S} \underset{\sim}{\boldsymbol{p}}_{s}^{d}\Big|_{r} \tag{2.19}$$

For each sub-period h, we approximate the *c.d.f.* $F_{\underset{\sim}{P}_{\Sigma}^{d}\,|_{h,r}}(\cdot)$ and its moments by using the sample space of $\underset{\sim}{\bar{\boldsymbol{P}}}^{d}\Big|_{r}$. In terms of the conditional probabilities, we state the *c.d.f.*

$F_{\underset{\sim}{P}^{d}_{\Sigma}\,|_{h}}(\cdot)$ to be:

$$
\begin{aligned}
F_{\underset{\sim}{P}^{d}_{\Sigma}\,|_{h}}(x) &= Prob\{\underset{\sim}{P}^{d}_{\Sigma}\,|_{h} \le x\} \\
&= Prob\{\underset{\sim}{P}^{d}_{\Sigma}\,|_{h} \le x \ on\ each\ \mathcal{R}_r\} \\
&= \sum_{r=1}^{R} Prob\{\underset{\sim}{P}^{d}_{\Sigma}\,|_{h,r} \le x\} Prob\{\mathcal{R}_r\} \\
&= \sum_{r=1}^{R} F_{\underset{\sim}{P}^{d}_{\Sigma}\,|_{h,r}}(x) \cdot \pi_r
\end{aligned}
\tag{2.20}
$$

Also, for the day *d*, we approximate the joint *c.d.f.* $F_{\underset{\sim}{\boldsymbol{P}}^{d}_{\Sigma}\,|_{r}}(\cdot,\cdot,\ldots,\cdot)$ for the *H* hourly values of $\underset{\sim}{\boldsymbol{P}}^{d}_{\Sigma}|_{r}$ – the sum of the conditioned *r.v.s.* $\underset{\sim}{\boldsymbol{P}}^{d}_{1}|_{r}$, $\underset{\sim}{\boldsymbol{P}}^{d}_{2}|_{r}$, …, $\underset{\sim}{\boldsymbol{P}}^{d}_{S}|_{r}$, which we use to compute the $F_{\underset{\sim}{\boldsymbol{P}}^{d}_{\Sigma}\,|_{r}}(\cdot,\cdot,\ldots,\cdot)$ with

$$
\begin{aligned}
F_{\underset{\sim}{\boldsymbol{P}}^{d}_{\Sigma}}(x_1, x_2, \ldots, x_H) &= Prob\{\underset{\sim}{P}^{d}_{\Sigma}\,|_{h} \le x_h, h = 1, 2, \ldots, H\} \\
&= \sum_{r=1}^{R} F_{\underset{\sim}{\boldsymbol{P}}^{d}_{\Sigma}\,|_{r}}(x_1, x_2, \ldots, x_H) \cdot \pi_r
\end{aligned}
\tag{2.21}
$$

The probabilistic characterization of the multi-site *CSP* resource power outputs in (2.16) – (2.21) is the foundation of the extension of the conventional probabilistic production simulation approach to represent the multi-site *CSP* power outputs in a system with integrated *CSP*s.

2.4. Summary

This chapter provides a description of the construction of a probabilistic model for the multi-site *CSP* resource power outputs, using sets of seasonal *DNI* data at the *S* sites with *CSP*s. We first formulate an optimization problem used to compute the multi-site *CSP* power outputs. Then we scale the seasonal daily *DNI* data into a common time scale so that we are able to compare the data of different days in a meaningful way. We classify the time-scaled *DNI* data into several clusters. For simulation purposes, we de-scale the samples drawn from each cluster and use them to compute the corresponding multi-site *CSP* power outputs for the day of interest. We use these samples to approximate the conditional distributions of the *CSP* output random variables.

In the next chapter, we provide a brief review of the conventional probabilistic production simulation approach and describe the steps needed to incorporate the multi-site *CSP* output model into the probabilistic production simulation framework.

3. THE EXTENSION OF PROBABILISTIC SIMULATION APPROACH

The probabilistic simulation approach is widely deployed in the evaluation of the expected energy production by each unit over a specified study period, the reliability metrics, the expected system production costs, the expected greenhouse gas emissions and any other metric of interest to measure the variable effects. The conventional probabilistic simulation is a computer-based emulation of the power system supply- and demand-side resource operations to assess how effectively the demand is met over a specified period. However, the conventional approach cannot represent time-varying resources such as *CSP*s. In this chapter, we review the probabilistic production simulation tool basics and discuss the necessary modifications to incorporate the model developed in chapter 2 to represent the integrated multi-site *CSP* resources. We also discuss some implementation aspects of the extended simulation approach.

3.1. Review of the Conventional Probabilistic Production Approach

To realistically emulate the operation of a power system, we decompose a multiple-year study horizon into W non-overlapping simulation periods. We specify each simulation period in such a way that no changes in the resource mix, unit commitment and the policy environment occur during its duration. Such changes may occur, however, in subsequent periods. We denote the index set of sub-periods in each simulation period by $\mathcal{T}$:

$$\mathcal{T} = \{1, 2, ..., T\} \tag{3.1}$$

For concreteness in this description, we choose a week as the simulation period and one hour as the smallest, indecomposable unit of time with T = 168 and H = 24. We illustrate the general structure of our scheme in Fig. 3.1. We note that the structure of the scheme is sufficiently general to accommodate any desired granularity.[†]

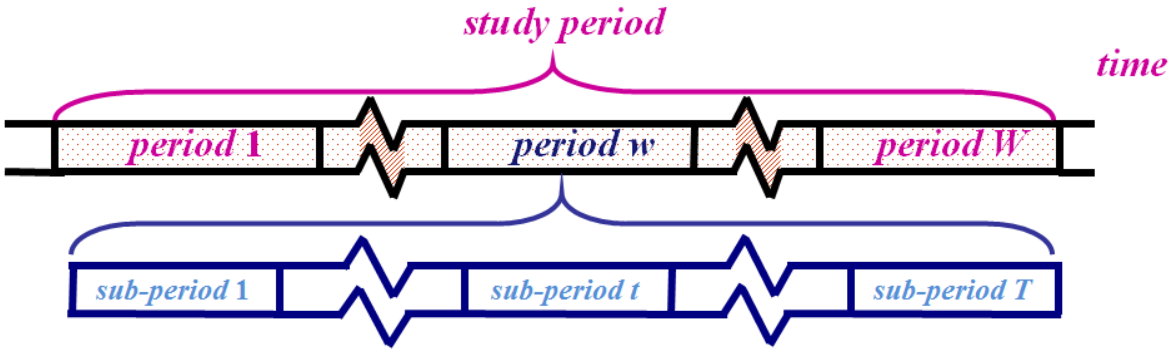

Figure 3.1: The general structure of the scheme based on the partitioning of the study period into W simulation periods, with each simulation period partitioned into T simulation sub-periods and each sub-period equal to the smallest, indecomposable unit of time

The load and resource characteristics, as well as the unit commitment in each simulation period are inputs into the simulation. Based on the chronological load data for the given simulation period, we develop a probability distribution to represent the load *r.v.* $\underset{\sim}{L}$. To do so, we ignore the time information and rearrange the loads in order of decreasing values from the highest to the lowest and construct the load duration curve (*l.d.c.*). The reordered load values contain no temporal information and all the inter-temporal effects are also lost in this representation. As an example, we plot in Fig. 3.2 the *ERCOT* chronological load data for Monday, July 25, to Sunday, July 31, 2011. We display in Fig. 3.3 the

[†] With the consideration of the thermal dynamic process, we adopt the granularity no less than 15 minutes as one sub-period. If, however, granularity smaller than 15 minutes is chosen for the simulation, the modifications of the *SP* are needed to take into account the dynamics of the thermal processes.

corresponding *l.d.c.*. We can identify the maximum/minimum load values from the *l.d.c.* during the simulation period. We interpret the *l.d.c.* as the complement of the *c.d.f.* of $\underset{\sim}{L}$. Consider an arbitrary point (ℓ, h) on the *l.d.c.*. We also interpret such a point as the statement that the load exceeds the value of ℓ for h hours during the T hours of the simulation period. The normalization of the time provides the fraction h/T, which we view to be the probability that the load exceeds the value ℓ in the simulation period. Thus, we use the inverted *l.d.c.* $\mathscr{L}$ to analytically characterize *c.d.f.* $F_{\underset{\sim}{L}}(\cdot)$ of $\underset{\sim}{L}$:

$$\mathscr{L}(\ell) = Prob(\underset{\sim}{L} \geq \ell) = 1 - Prob(\underset{\sim}{L} \leq \ell) = 1 - F_{\underset{\sim}{L}}(\ell) \tag{3.2}$$

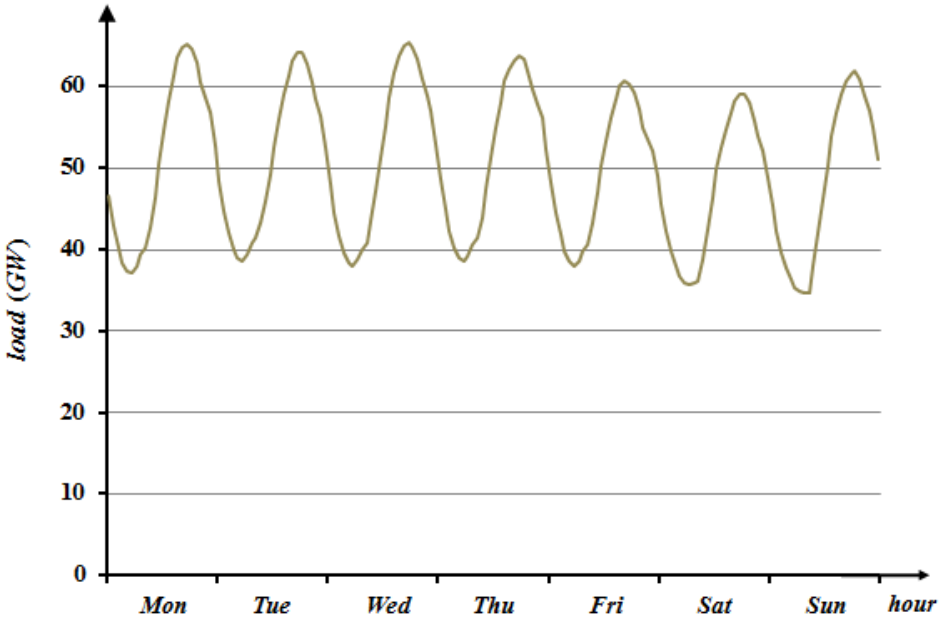

Figure 3.2: The *ERCOT* system chronological hourly load from Monday, July 25, to Sunday, July 31, 2011 [18]

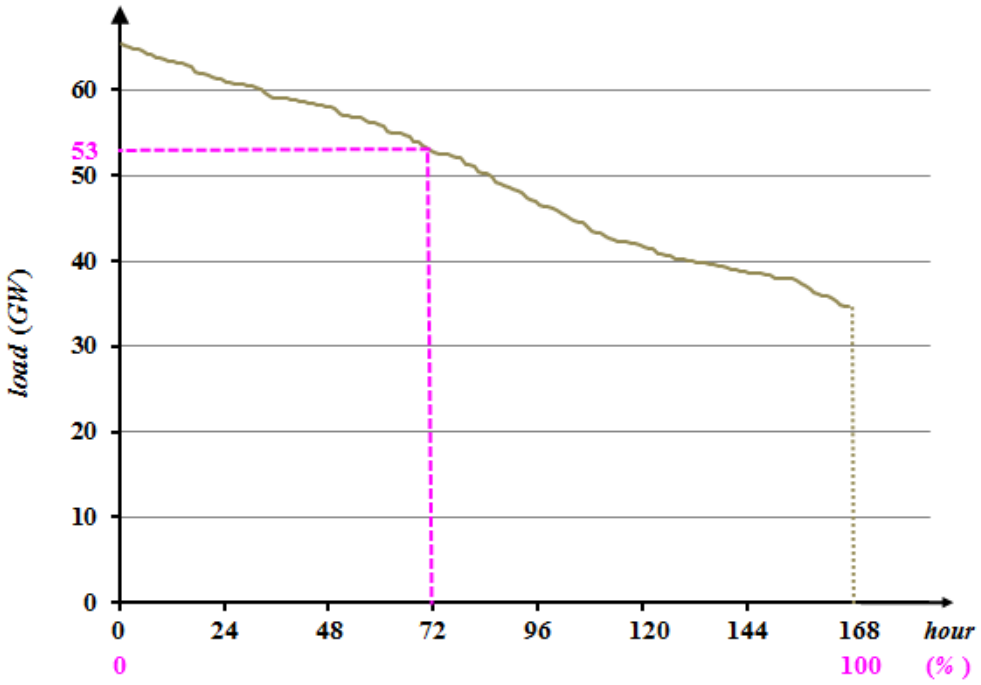

Figure 3.3: The *l.d.c.* for Monday, July 25, to Sunday, July 31, 2011.

A unit generates energy to serve the load, once it is committed and dispatched [29]. In each simulation period w, $\mathscr{E}^w$ is the index set of the committed conventional units and can be viewed as a subset of the $\mathscr{E}$ – the set of conventional generation units, where:

$$\mathscr{E} = \{i,\ i = 1,\ 2, ..., |\mathscr{E}|\} \tag{3.3a}$$

$$\mathscr{E}^w = \{i : 1 \le i \le |\mathscr{E}| \text{ and unit } i \text{ is committed in simulation period } w\} \tag{3.3b}$$

We model the availability of each controllable unit by its multi-state available capacity *r.v.* [29]. Each unit may be represented by a single-block or a multi-block model. The blocks of the committed units in $\mathscr{E}^w$ are loaded to meet the load in the order of their non-decreasing marginal prices during the period w. In this way, we construct the period w loading order

of committed units and we refer to this order as the loading list. The probabilistic simulation approach uses the notion of the equivalent load *r.v.* $\underset{\sim}{L}_k$ – the remaining uncertain load served by the blocks in the loading list after the first $k-1$ blocks are loaded. The recursive relation

$$\underset{\sim}{L}_k = \underset{\sim}{L}_{k-1} - \underset{\sim}{A}_k \quad \textit{with} \quad \underset{\sim}{L}_0 = \underset{\sim}{L} \tag{3.4}$$

computes the equivalent load *r.v.* $\underset{\sim}{L}_k$ iteratively, where $\underset{\sim}{A}_k$ represents the available capacity *r.v.* of the loading block *k*. We assume that each unit is independent of each other unit and the load, and compute the $\mathscr{L}_1$, $\mathscr{L}_2$, … functional values rapidly by convolution to evaluate the variable effects of the power system in each simulation period. Here, $\mathscr{L}_k$ is the inverted *l.d.c.* corresponding to the equivalent load *r.v.* $\underset{\sim}{L}_k$. As an example, we use $\mathscr{L}_{k-1}$ to determine the expected energy production ε_k of loading block *k* over the simulation period:

$$\varepsilon_k = \int_{C_{k-1}}^{C_k} \mathscr{L}_{k-1}(\ell)\, d\ell \tag{3.5}$$

with

$$C_k = \sum_{q=1}^{k} c_q \qquad k = 1, 2, \ldots \tag{3.6}$$

where c_q is the capacity of the block *q*.

Given the heat rate and fossil fuel data for each loading block *q*, we can compute the block *k* expected production costs and emissions during the simulation period. In addition,

the production simulation also provides, as a byproduct, the values of the system reliability metrics of interest. Since the *l.d.c.* of the equivalent load *r.v.* after all the blocks are loaded provides the complement of the *c.d.f.* of the load that remains unserved, we can derive the relations to determine the *loss of load probability* ($LOLP^w$) and the *expected unserved energy* (EUE^w) by:

$$LOLP^w = \mathscr{L}_{K^w}\left(C_{K^w}\right) \tag{3.7}$$

$$EUE^w = \int_{C_{K^w}}^{+\infty} \mathscr{L}_{K^w}(\ell)\, d\ell \tag{3.8}$$

where K^w is the number of blocks loaded during the simulation period *w*. We make use of (3.7) and (3.8) in the evaluation of the metrics of interest.

3.2. Reexamination of the Load Representation

To mesh the probabilistic simulation framework with the probabilistic model of the multi-site *CSP* power outputs, we need to reexamine the load sample space. In each weekly simulation period, we collect the *H* daily load values to construct the load *r.v.* sample space of the *T* load values, where *T* is the total number of sub-periods in the simulation period. We use the aggregated *CSP* power output *r.v.* $\underset{\sim}{P}_{\Sigma}^{d}\Big|_{h}$ in each sub-period *h* to meet part of the corresponding load of the sub-period. To do so, we partition the load *r.v.* sample space into *H* non-overlapping subsets, with each subset containing realizations of the load *r.v.* conditioned on the sub-period *h*. Consequently, we may view the sample space as a

matrix with D rows and H columns. Let $\mathcal{T}|_1, \mathcal{T}|_2, \ldots, \mathcal{T}|_H$ be the H subsets of $\mathcal{T}$, with each subset $\mathcal{T}|_h$ being a subset of the indices, one for each day, of the sub-period h for the D days in the simulation period w. Thus, we write

$$\mathcal{T} = \bigcup_{h=1}^{H} \mathcal{T}|_h \tag{3.9}$$

$$\mathcal{T}|_h \cap \mathcal{T}|_{h'} = \varnothing \quad for \quad h \neq h' \tag{3.10}$$

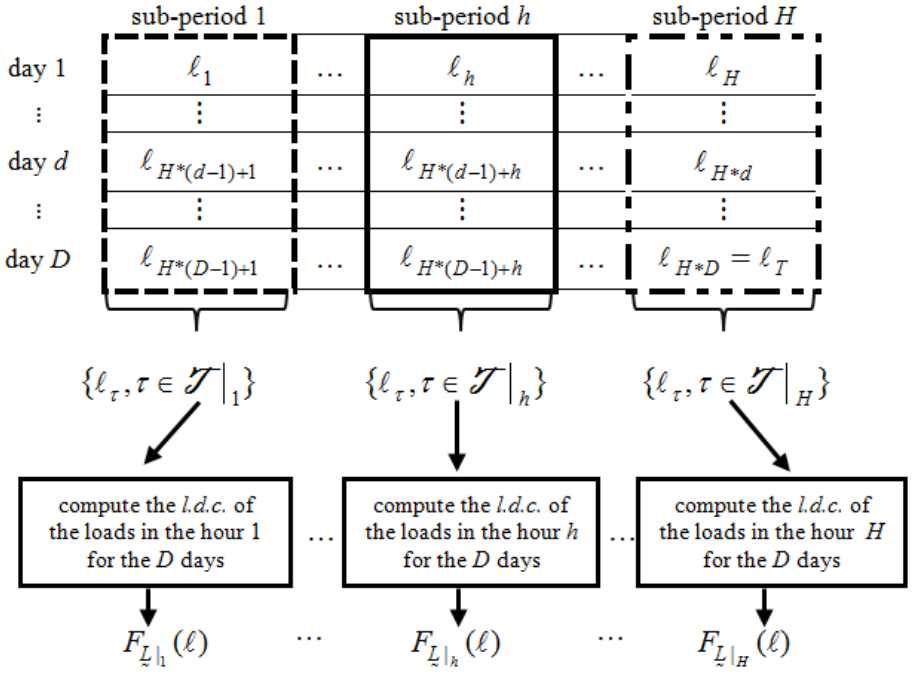

Figure 3.4: The load representation for the partitioned *r.v.* sample

We use the samples in the set $\{\ell_j,\ j \in \mathcal{T}|_h\}$ to approximate the *c.d.f.* $F_{L|_h}(\ell)$ of the load *r.v.* conditioned on the sub-period h. We summarize in Fig. 3.4 the visualization of the

load *r.v.* sample space partition we use in this analysis. Since each of the H non-overlapping subsets has an equal probability $1/H$, the application of conditional probability allows us to restate the *c.d.f.* $F_{\underset{\sim}{L}}(\cdot)$ of $\underset{\sim}{L}$ in terms of the conditioned *c.d.f.*s of $\underset{\sim}{L}\,\big|_h$. Thus,

$$\begin{aligned} F_{\underset{\sim}{L}}(\ell) &= Prob\{\underset{\sim}{L} \le \ell\} \\ &= Prob\{\underset{\sim}{L} \le \ell \text{ in each sub-period } h\} \\ &= \sum_{h=1}^{H} Prob\{\underset{\sim}{L} \le \ell \,|\, hour\ h\} Prob\{hour\ h\} \\ &= \frac{1}{H}\sum_{h=1}^{H} F_{\underset{\sim}{L}|_h}(\ell) \end{aligned} \tag{3.11}$$

Under the assumption that each unit has uniform characteristics during the entire simulation period, we express the *c.d.f.* $F_{\underset{\sim}{L}_k}(\ell)$ of the equivalent load *r.v.* $\underset{\sim}{L}_k$ similarly in terms of the conditioned *c.d.f.*s of $\underset{\sim}{L}_k\,\big|_h$. In this way,

$$F_{\underset{\sim}{L}_k}(\ell) = Prob\{\underset{\sim}{L}_k \le \ell\} = \frac{1}{H}\sum_{h=1}^{H} F_{\underset{\sim}{L}_k|_h}(\ell) \tag{3.12}$$

where $F_{\underset{\sim}{L}_k|_h}(\ell)$ denotes the probability of the equivalent load *r.v.* conditioned on the sub-period h. We restate all the probabilistic simulation relations in terms of the conditional probability with the conditioning on the sub-period h of each day in the simulation period.

3.3. Extension of Production Simulation with Time-Dependent Resources

We incorporate the representation of the multi-site *CSP* resource impacts by making use of the load sample space partitioning in combination with the regime-based multi-site *CSP* power outputs. The multi-site *CSP* power output *r.v.* meets some of the demand, with the conventional controllable resources serving the other part. We use the term "controllable load" $\tilde{C}$ to represent the remaining "net" load *r.v.* that is met by the conventional units, explicitly taking into account the output provided by the *CSP*s. We use the conventional assumption that the load and multi-site *CSP* power output *r.v.*s are statistically independent. We approximate the *c.d.f.* $F_{\tilde{C}|_{h,r}}(\cdot)$ of the controllable load *r.v.* conditioned on the cluster $\mathcal{R}_r$ for the sub-period *h* making repeated use of the convolution operation. We then restate the *c.d.f.* $F_{\tilde{C}|_{h,r}}(\cdot)$ of the controllable load *r.v.* conditioned on the cluster $\mathcal{R}_r$ as:

$$F_{\tilde{C}|_r}(c) = Prob\{\tilde{C} \le c \,|\, \mathcal{R}_r\} = \frac{1}{H}\sum_{h=1}^{H} F_{\tilde{C}|_{h,r}}(c) \tag{3.13}$$

Once the approximation of $F_{\tilde{C}|_r}(\cdot)$ for a regime *r* is obtained, the probabilistic simulation for the controllable resources proceeds exactly as under the conventional case. The expected value of each metric of interest in a simulation period is evaluated as the cluster-probability-weighted average of the conditional expected values.

For the entire study period, the expected value of each metric, such as a reliability index, an economic measure or an environmental emission value, is computed as the sum of the expected values in each simulation period.

3.4. Summary

In this chapter, we present a review of the probabilistic production simulation framework for systems whose resource mix is constituted only of controllable units. We devote the rest of this chapter to discuss the extension of its capability to explicitly include the representation of *CSP* resources. We modify the load representation so that it is compatible with the regimes-based *CSP* power probabilistic representation developed in Chapter 2. In the next chapter, we discuss the application of the extended probabilistic simulation approach to assess the variable effects of systems with integrated *CSP* resources.

4. ILLUSTRATIVE SIMULATION RESULTS

The extended probabilistic approach has a wide range of applications, including resource planning, production costing issues, environmental assessments, reliability and policy analysis. We carried out extensive simulation studies with the extended probabilistic approach and devote this chapter to presenting representative results that illustrate the capabilities of the approach to quantify the variable effects of a system with integrated multi-site *CSP* resources. We start out with a description of the test system characteristics used in the representative studies discussed here. We present the results of the four study sets selected for the discussion in this chapter. In the study set I, we focus on the investigation of the impacts of deepening *CSP* penetration. We discuss the impacts of the *TES* capability in the study set II. The study set III results provide insights into the capability of the multi-site *CSP*s to replace the retired conventional generation capacity. We analyze the impacts of two different *TES* operational objectives on the simulation results for the study set IV.

4.1. The Test System and the Simulation Parameters

We use a single test system for the four study sets reported in this chapter. In our discussion, each simulation study is considered for the year 2004 so as to focus on the nature of the results and the insights they provide. The test system is a modified version of *WECC* 240-bus system [30]. The test system represents only the resources and loads without the network. We scale the 2004 *WECC* load data so that the annual peak load is 81,731 MW. The test system has 902 conventional generation units with a total nameplate capacity of 96,443 MW and we explicitly represent the unit maintenance schedule. The

reserves are maintained at 15 % level throughout the year. We use the outage probability and the economics of every block for each conventional unit from [30]. The fuel costs and CO_2 emission rate data are also those given in [30]. Each case study considers *CSP*s with equal capacity installed at six selected sites. The six sites selected for the *CSP*s are all on the *WECC* footprint, namely Barstow, Blythe and Lancaster in California, Lovelock and Mercury in Nevada, and Tucson in Arizona. Each *CSP* uses the parabolic trough structure with a solar multiple of 2. We use historical *DNI* measurement data with $M = 24$ from 2002 – 2004 [31] to identify the *DNI* clusters for our studies. We assume that each *TES* is operated to maximize the total energy production of the aggregated *CSP* units. For the *SP* objective function, each coefficient $\gamma_s^d[h]$ is assumed to be 1.

We partition the 52 weeks of the study year into four seasons and use one hour as the smallest indecomposable unit of time for each day with $H = 24$. Given the importance of the J value in the *DNI* pattern representation, the J choice involves a trade-off between the accuracy of the solar pattern representation and the computational burden. We determine the J value from a sensitivity study over the [0,100] interval. For each value of J, we scale and then descale *DNI* data and evaluate the average absolute difference between the descaled *DNI* data and its measured value expressed in per unit of the measured *DNI* value. For the specified M and H values, we plot in Fig. 4.1 the average error for the range of study for J. As J increases, the average error decreases. In our simulations, we use $J = 80$ to obtain an average error at or below 1 % level for the equal-duration common time-scaled sub-periods in the *CSP* model.

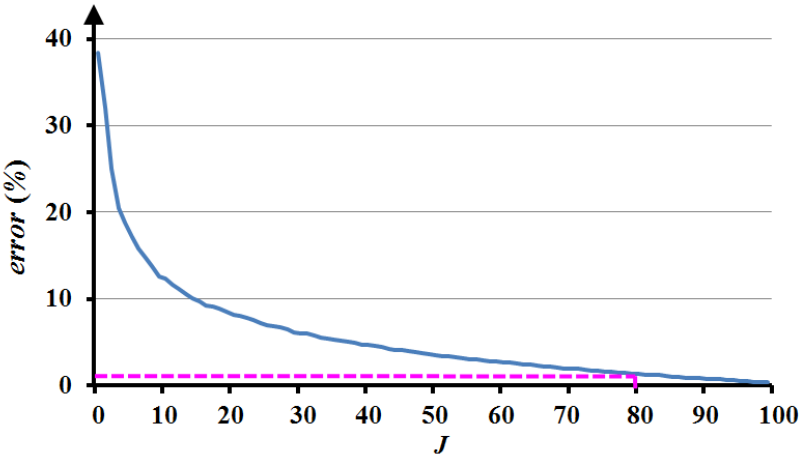

Figure 4.1: The average error as a function of J

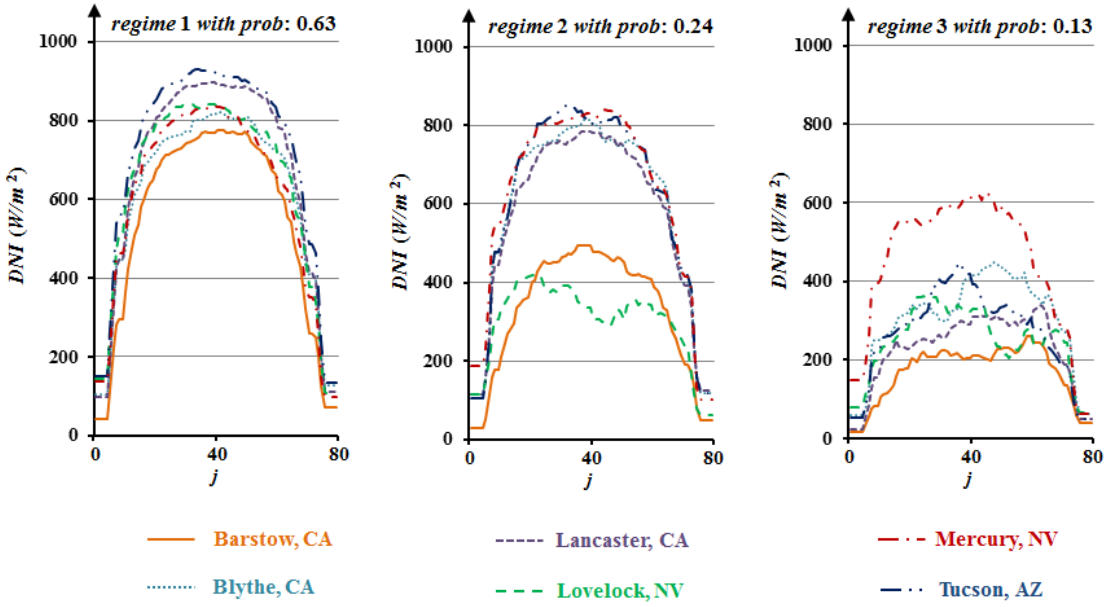

Figure 4.2: The centroids (J = 80) of *DNI* regimes for R = 3, using k-means clustering algorithm for the autumn season at the six sites selected for simulation

An important parameter to be determined is the number of regimes to use in the *DNI* representation. To gain some insights into the value of R, we scale the 2002 – 2004 data

and classify them into a specified number R of clusters, with R = 3, 4, 5. We display the corresponding results for the autumn season in Fig 4.2 – 4.4, respectively. We plot the patterns of each regime and provide the probability of each regime for each R we choose. We note that for the autumn season at least one regime has a probability smaller than 0.10 when R exceeds 4, and that there is one dominant regime with probability higher than 0.6 when R is less than 4. Based on these results, we can obtain an acceptable approximation of the *DNI* uncertainty with R = 4. All the studies discussed in this chapter are obtained with R = 4 for each season.

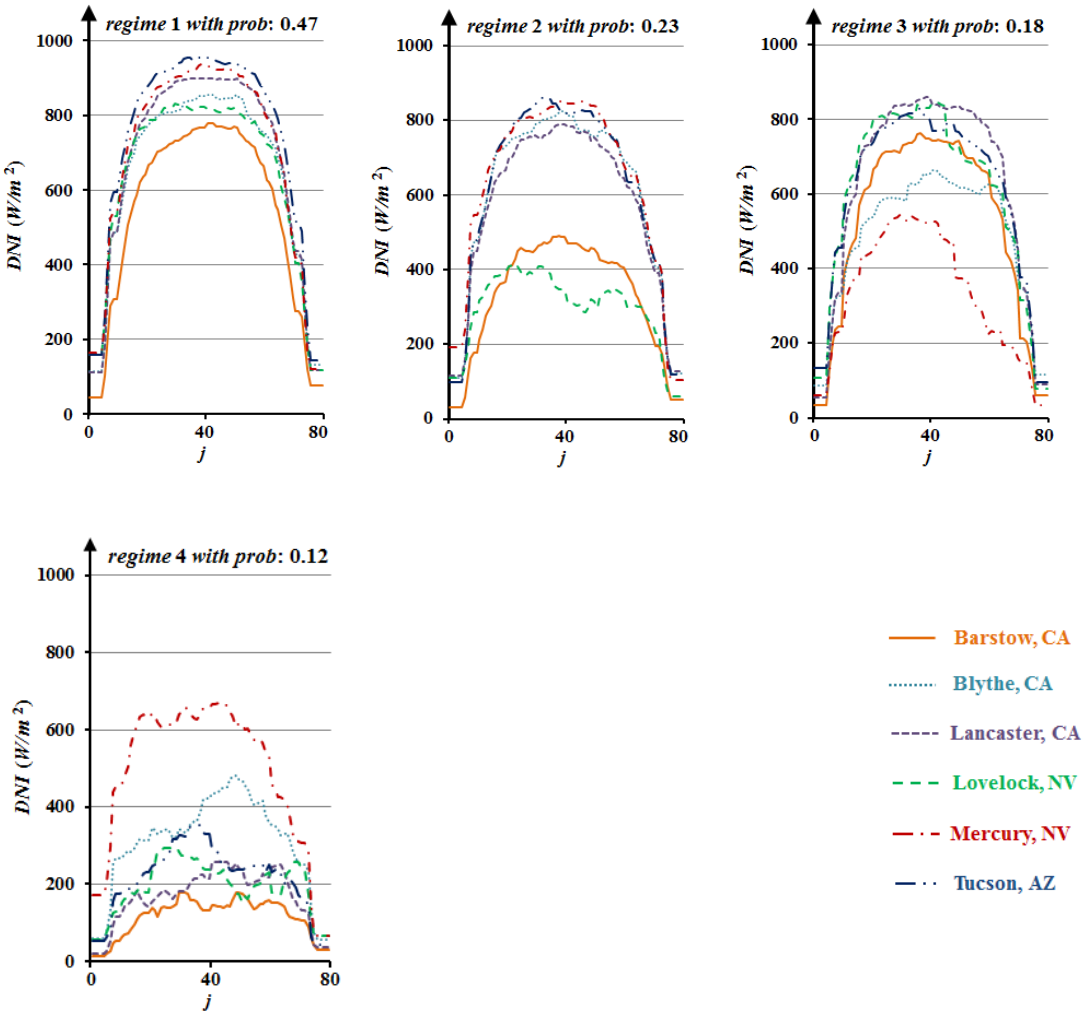

Figure 4.3: The centroids (J = 80) of *DNI* regimes for the autumn season with R = 4

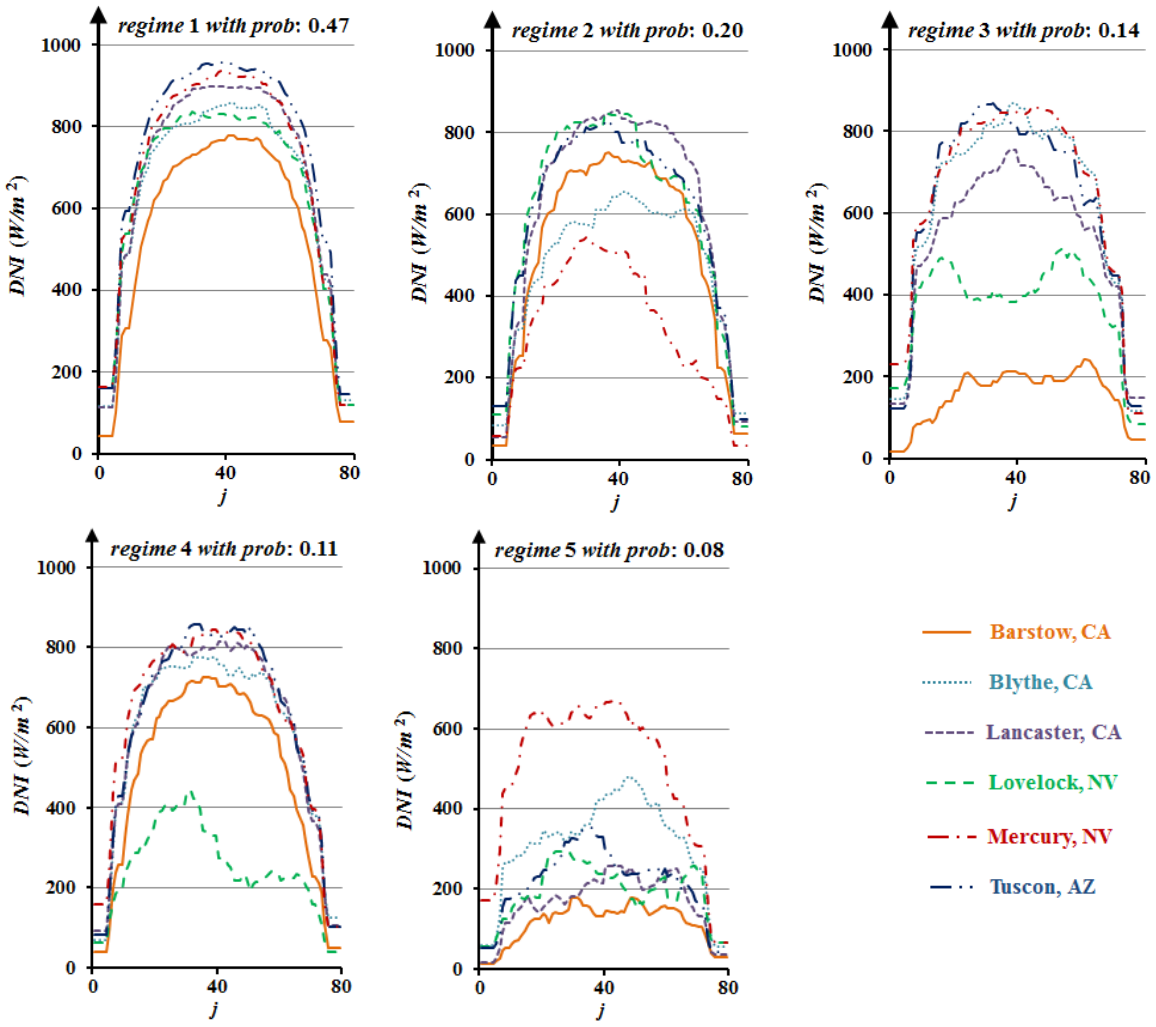

Figure 4.4: The centroids (J = 80) of *DNI* regimes for the autumn with R = 5

4.2. Study Set I: Impacts of the Deepening *CSP* Penetration

In the study set I, we use the test system with varying amounts of the total installed *CSP* capacity from 0 MW – the base case – to 3,000 MW in 600-MW increments with a 1-hour *TES* capability at each *CSP*. We start out the discussion of the results of study set I with the base case for the supply system consisting only of the controllable conventional resources.

We summarize in Table 4.1 the values of the reliability metrics – the *LOLP* and the *EUE* – and the expected production costs and the CO_2 emissions for the single year period.

Table 4.1: Simulation results for study set I base case

metric	*LOLP*	*EUE* (MWh)	expected production costs ($)	expected CO_2 emissions (lbs)
value	1.12×10^{-3}	253	1×10^{10}	3×10^{11}

We next discuss the sensitivity cases with increments of the *CSP* capacity. For each case, we evaluate metrics of interest and their percentage changes *w.r.t.* the base case results. We display the results in Fig. 4.5. The *LOLE* and *EUE* reductions reflect the reliability improvements in the system due to the multi-site *CSP* integration. The results clearly indicate the diminishing returns in the reliability improvements: although the *CSP* integration with higher total capacity further reduces the *LOLP* and the *EUE* values, the reliability improvement of each successive capacity increment has smaller impacts than the preceding increment. In addition, we note that the annual expected production costs and CO_2 emissions decrease almost linearly as the total *CSP* capacity increases. Such results are reasonable since every additional unit of the *CSP* generation displaces the energy produced by the more costly and polluting units. The production costs and CO_2 emissions of each conventional unit are assumed to be linearly dependent on the unit energy production and so the annual expected production costs and CO_2 emissions behave accordingly. Similar behavior in reliability improvements, costs and CO_2 emissions is also evident in the wind and *PV* resource integration studies performed earlier [29], [26].

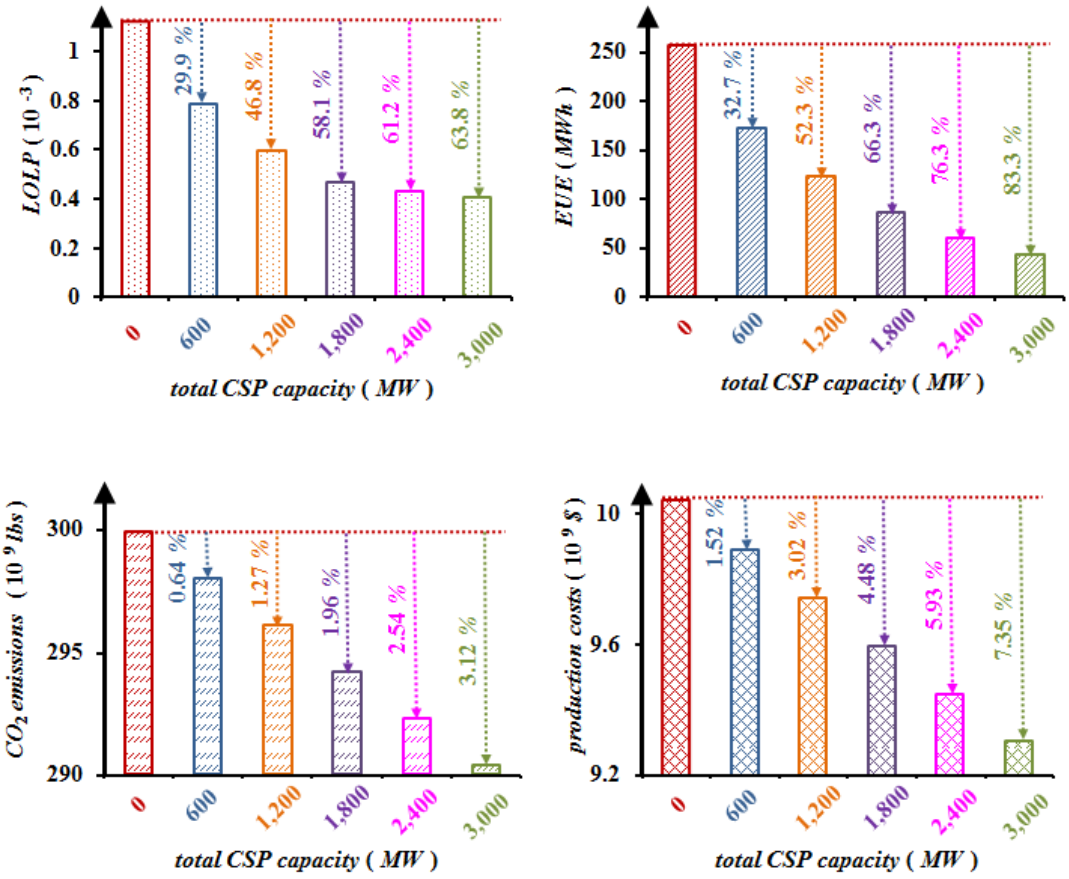

Figure 4.5: The annual value of each metric with the corresponding percentage change *w.r.t.* the base case value for the *CSP* penetration sensitivity study for installed *CSP* capacity from 0 – 3,000 MW

We focus on the simulation results for four seasons for the case with 1,200-MW *CSP* resources and examine the relationship of the annual metric values to their seasonal components. In Table 4.2, we give the simulation results for the four seasons and also for the entire year. Since summer has the highest energy demand, the *LOLP* in the summer is almost 100 times of that of the spring season. The expected CO_2 emissions in the winter are 10 % lower than those in the summer. These simulation results are representative of the

general nature of these metrics and explicitly demonstrate the seasonal variations of reliability and economic impacts of the integrated *CSP* resources and the relative influence of each season.

Table 4.2: Seasonal and yearly values of the metrics of interest for the case with 1,200-MW *CSP* capacity

metric	season				entire 2004 year
	spring	summer	autumn	winter	
LOLP (10^{-4})	0.16	15.9	5.23	2.92	6
EUE (MWh)	1.8	112.4	8.2	0.6	123
production costs (10^{9} \$)	2.43	2.60	2.47	2.24	9.74
expected CO_2 emissions (10^{10} lbs)	7.91	7.34	7.72	6.60	29.6

We next explore the impacts of *DNI* regime in the evaluation of the metrics of interest. We display in Table 4.3 the metric values for the summer season conditioned on the cluster $\mathcal{R}_r$, r = 1, 2, 3, 4, together with the regime probability weighted average. From these results, it follows that the metrics have markedly different contributions for each regime to the metrics in the summer period. For instance, the *LOLP* conditioned on cluster $\mathcal{R}_4$ is about 23 % larger than the *LOLP* conditioned on cluster $\mathcal{R}_1$. This is because those daily *DNI* patterns in cluster $\mathcal{R}_1$ represent the *DNI* pattern with the higher solar energy content. The simulation results clearly illustrate the strong dependence of reliability and economic

impacts of the *CSP* resources on the different daily *DNI* patterns. However, we also note the trivial contribution of *LOLP* and *EUE* values conditioned on cluster $\mathcal{R}_4$ to the system overall *LOLP* and *EUE* values. This is because the overall metric value is the weighted average of the results conditioned on each cluster. Compared to other three clusters, the cluster $\mathcal{R}_4$ has a lower probability and so has a smaller contribution to the system overall reliability metric values. Thus, the product of a metric conditioned on each cluster with the cluster's probability determines the contribution of each cluster to the overall value of the metric.

Table 4.3: Seasonal simulation results for the summer in case with 1,200-MW *CSP*s

metric	regime				summer
	$\mathcal{R}_1$	$\mathcal{R}_2$	$\mathcal{R}_3$	$\mathcal{R}_4$	
LOLP (10^{-4})	15.5	16.4	15.9	19.1	15.9
EUE (MWh)	107	114	109	131	112.4
production costs (10^{9} \$)	2.59	2.60	2.59	2.63	2.61
expected CO_2 emissions (10^{10} lbs)	7.33	7.44	7.39	7.38	7.34

In study set I, we observe the greater contributions of the *CSP* resources to the system with significantly diminishing returns as their installed capacity increases. For a fixed installed *CSP* capacity, seasonal variations are noted in the values of each metric of interest in the four seasons of the year. Those variations indicate that each of the four seasons

poses different challenges for system operations, reliability and economic effects. Additionally, the simulation results in each of the regimes demonstrate that regime-based representation effectively captures the variations for different *DNI* pattern clusters and their contributions to each metric.

4.3. Study Set II: Sensitivity of the *TES* Capability

For the study set II, we fix the total installed *CSP* capacity in the test system at 1,200 MW. Our focus is on the impacts of the *TES* capability as it varies from 0 hour – the base case – to 6 hours, in 1-hour increment increases. These increments are applied at all the sites in a uniform way. The base case metric results are presented in Table 4.4.

Table 4.4: Annual metric values for the study set II base case

metric	*LOLP*	*EUE* (MWh)	expected production costs ($)	expected CO_2 emissions (lbs)
value	6.4×10^{-4}	135	9.77×10^{9}	2.97×10^{11}

We next consider the sensitivity results for each capability increment. We present in Fig. 4.6 the percentage changes in the value of each metric *w.r.t.* the base case. As the *TES* capability increases and more thermal energy can be stored during the insolation hours for later conversion into electricity, the expected value of each metric decreases. However, the impacts of each successive capability increment become smaller and for the reliability

metrics, an increment above 4 hours results in a negligibly small change. This result is due to the fact that the solar energy in each day is insufficient for the *CSP* to take full advantage of the larger capability *TES*.

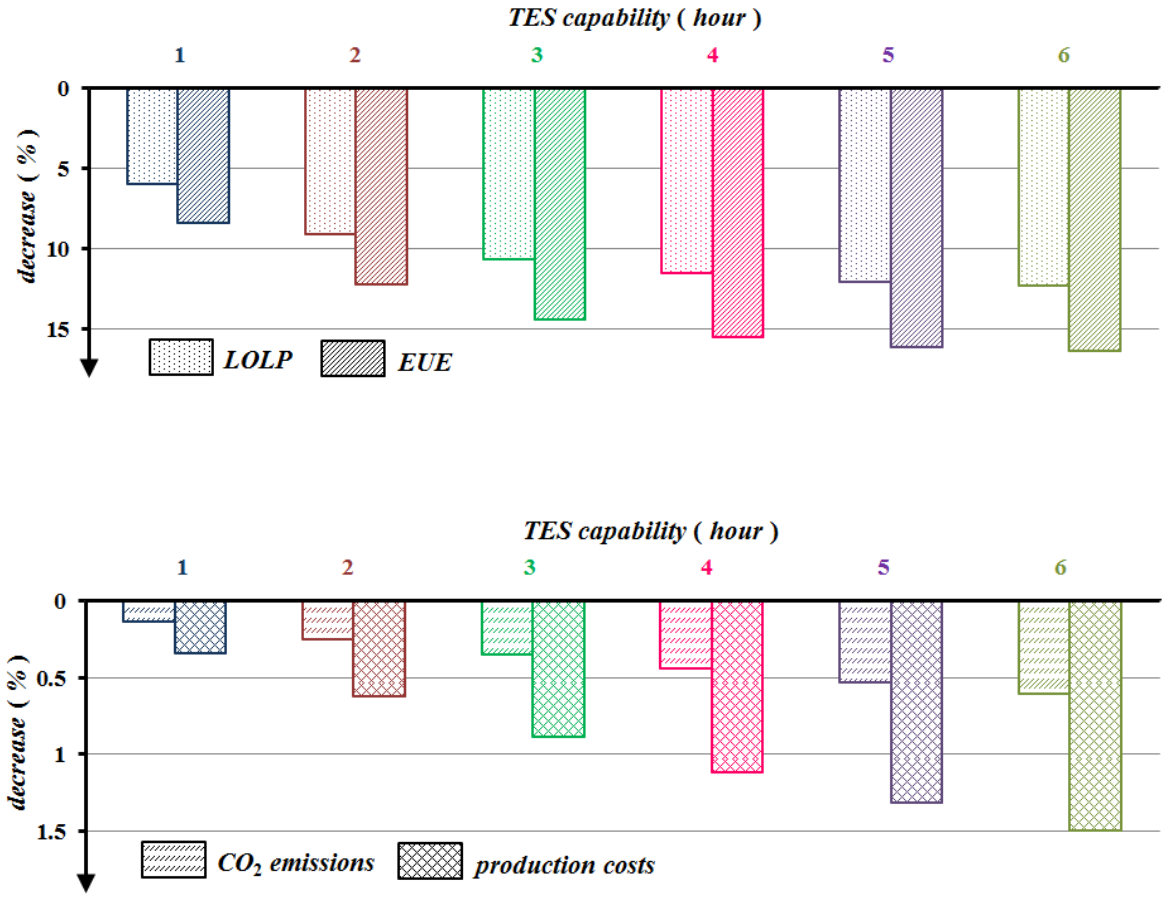

Figure 4.6: The percentage changes in the expected value of each metric *w.r.t.* the base case value for the *TES* capability sensitivity study

We discuss a second sensitivity study on *TES* capability in which we investigate the impacts of the choice of location of a *CSP* installation. The *CSP* capacity of each site is set

at 200 MW. In each case, we perform a simulation study with the *CSP*s sited at only 5 out of the 6 locations. The *CSP* resource at one of the three sites – Barstow, Blythe and Lancaster – is not installed. Each simulation is run with the *TES* capability from 0 to 4 hours for 200-MW *CSP* at each of the 5 sites. We display the results for *LOLP* and CO_2 emissions in Fig. 4.7 and also include for comparative purposes the results for the case with the *CSP* at each of the six sites. The behavior of these two metrics of interest in the sensitivity study cases under different *TES* capability values is quite similar. We note that, among the three possible sites without a *CSP* installation, the *CSP* resource installed at Blythe has the most marked impacts on the annual *LOLP* and the expected CO_2 emission values. Such results indicate clearly that the Blythe site has more solar energy, on average, for the *CSP* to harness than that in either the Barstow or the Lancaster sites. Consequently, the *TES* capacity investment at Blythe results in greater benefits to the multi-site *CSP* installation than that at either Barstow or Lancaster.

From the simulation results of study set II, we note that the installation of the *TES* enables *CSP*s to harness more solar energy so as to further improve the system reliability and reduce more emissions. However, it is not cost-effective to expand *TES* once *TES* capability reaches a threshold level because solar energy harnessable by the *CSP* cannot take full advantage of the *TES* with the larger capability. We also observe the strong location-dependence of the reliability metrics and CO_2 emissions under various *TES* capability conditions.

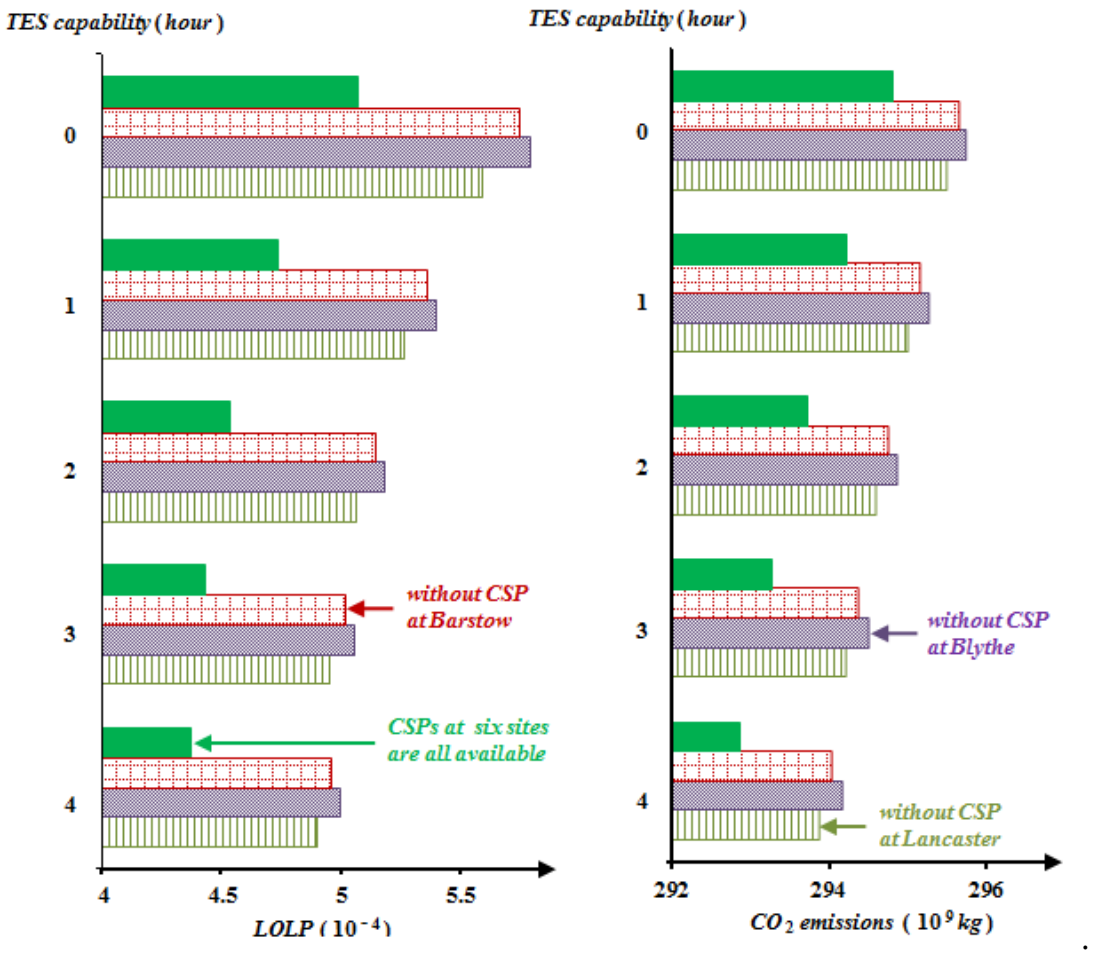

Figure 4.7: The *LOLP* and annual expected CO_2 emissions in the sensitivity study of the site choice for *TES* installation

4.4. Study Set III: Investigation of the Multi-site *CSP* Resource Ability to Replace Retired Conventional Unit Capacity

For the study set III, our aim is to investigate the ability of the multi-site *CSP* resources to replace retired conventional unit capacity from a purely reliability point of view. The base case of this study set is the test system without any *CSP* resource with the supply system consisting of all the controllable conventional units. We study the replacement of

1,000-MW conventional unit capacity by the multi-site *CSP* resources for each 120-MW increment of the total *CSP* capacity from 600 to 3,000 MW. We compute the *LOLP* and *EUE* for each additional increment. To gain some insights into the impacts of the *TES* capability, we perform each case with and without a 3-hour *TES* at each site. For the results shown in Fig. 4.8 and 4.9, we deduce that the 2,520-MW total *CSP* capacity without *TES* is able to replace the 1,000-MW conventional generation capacity with the annual *LOLP* and *EUE* remaining unchanged from the base case values. Without *TES*, the multi-site *CSP* resources have a much weaker ability to replace the retired conventional unit capacity from a purely reliability point of view. A similarly weak ability of wind resources to replace the retired conventional generation capacity is reported in [32]. With all other conditions remaining unchanged, the 3-hour *TES* reduces the needed total *CSP* capacity to 1,800 MW – about a 30 % reduction in capacity. Such a reduction in the installed *CSP* capacity indicates the *TES* "value" added to the multi-site *CSP* resource installation from a purely system reliability viewpoint.

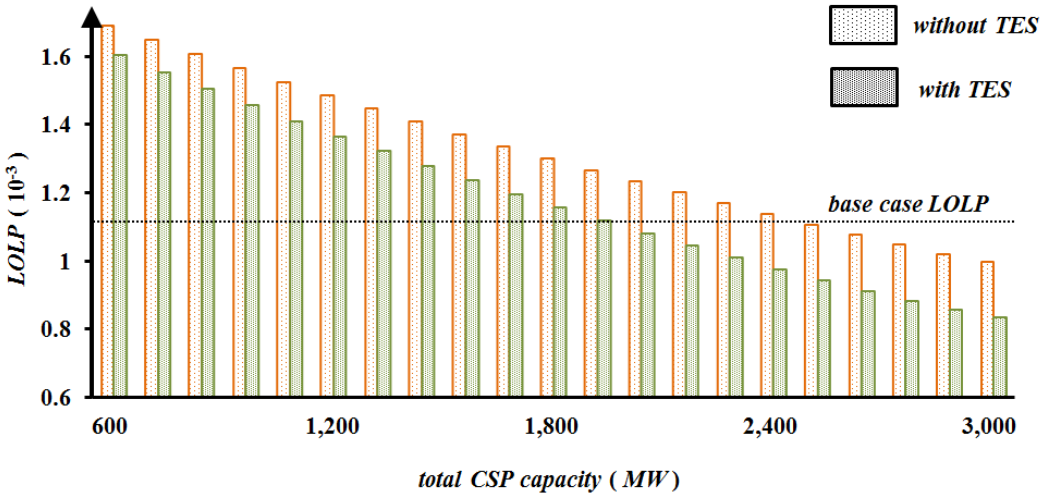

Figure 4.8: The annual *LOLP* metric values with/without the 3-hour *TES* for the set III sensitivity study

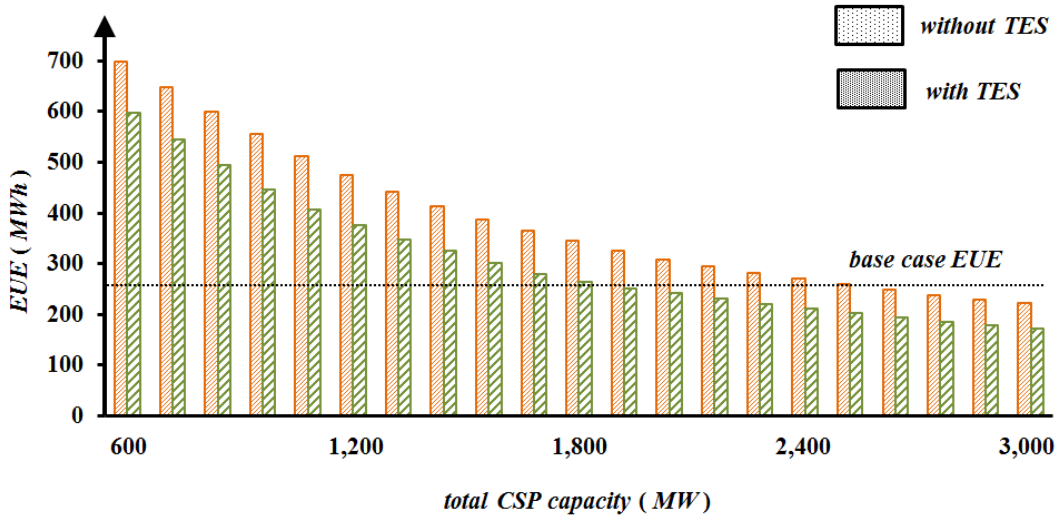

Figure 4.9: The annual *EUE* metric values with/without the 3-hour *TES* for the set III sensitivity study

Based on the reliability metrics in study set III, we conclude that the *CSP* resources without *TES* have weak ability to substitute for the retired generation capacity of conventional units. The incorporation of *TES* devices can improve considerately this ability of *CSP* resources and result in a reduced *CSP* capacity to replace the retired conventional unit capacity.

4.5. Study Set IV: Comparison of Two Different *TES* Operational Objective Impacts on the Power Systems

The purpose of the study set IV simulations is to compare the impacts of two different *TES* operational objectives at the multi-site *CSP* on the system variable effects. To make the investigation meaningful in light of the limited controllability of the *CSP*s without *TES*,

we consider the test system with 1,500-MW total installed *CSP* capacity with 3-hour *TES* at each location with the installations located at only three California sites: Barstow, Blythe and Lancaster. We compare the results of two case studies: in case 1, the objective is to maximize the total *CSP*-produced energy, and in the case 2, the objective is to maximize the total *CSP*-produced energy revenues based on forecasted system marginal prices. We treat case 1 as the base case and compare the values of the metrics of interest, as well as the additional metric that measures the costs of the *CSP* energy production under the two objectives. We normalize all metrics *w.r.t.* the base case values and display the results in Fig. 4.10.

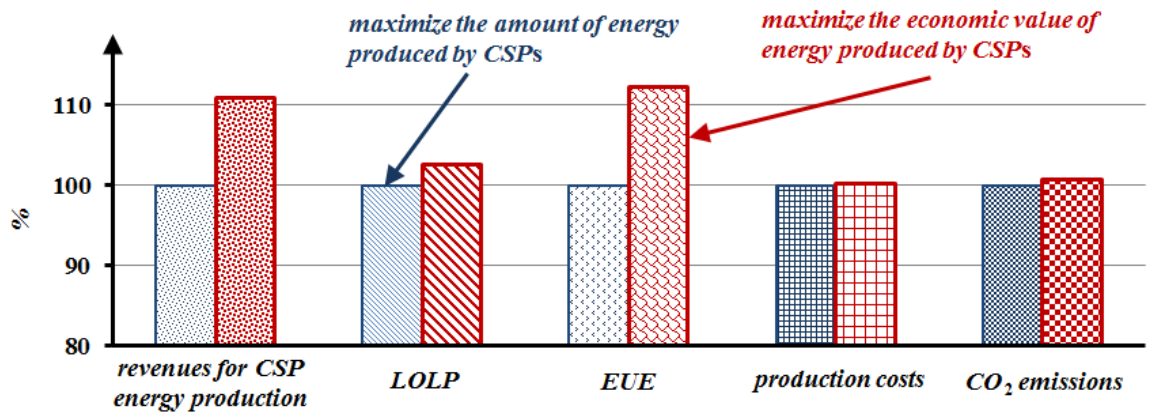

Figure 4.10: Comparison of the metric values for the cases of energy maximization (base case) and revenue maximization for the study set IV

The results in case 1 objective use forecasts of system marginal prices for each hour of the simulation period. Under the objective in case 2 to maximize the *CSP* revenues for energy production, the contribution of the multi-site *CSP* resources leads to poorer reliability, higher production costs and higher CO_2 emissions than those under the

objective in case 1 to maximize the total *CSP* energy production. While the *CSP* owner receives higher revenues under the case 2 objective for the postulated system marginal price forecasts, the system is overall worse off. In the objective of case 1, the maximization assumes that each unit of energy has exactly the same economic value – no time differentiated system marginal prices as under the case 2 objective. The losses over time in the energy stored in the *TES* contribute to the reduction of benefits to the system under the case 2 optimization.

The study set IV simulations under the two different *TES* operational objectives provide insights into the importance of the selected objective. The choice of operational objective for a *CSP* has impacts on the overall system benefits gained from *CSP* resources. Because different objective functions may produce different results, the *CSP* owner faces a trade-off between the improved reliability, environmental metric values of the system and the higher revenues for *CSP*-produced energy.

4.6. Summary

In this chapter, we discussed the results of our investigations of the impacts of the *CSP* resource spatial and temporal variability on the power system. We have shown the extent to which the integrated *CSP* resources and the incorporated *TES* result in an increase in the reliability and a reduction in the production costs and in the emissions of the power system. We have noted that the site choice for *CSP* installation is an important factor when investors decide to develop *CSP* resources. We have also quantified the replacement ability

of the multi-site *CSP* resources with explicit consideration of the variability and intermittency effects of solar energy.

5. CONCLUSION

In this chapter, we summarize the work presented in this thesis and identify directions for future work.

5.1. Summary

In this thesis, we presented the development and testing of an extended probabilistic simulation approach to assess, over longer-term periods, the variable effects of systems with integrated multi-site *CSP* resources. Throughout the thesis, we described in detail the successive steps essential to extend the conventional production simulation framework for systems with integrated multi-site *CSP* resources. We also present some of the simulation results we obtained from extensive study so as to demonstrate the capabilities of the extended tool and the usefulness of our work.

We started with the construction of the deterministic multi-site *CSP* power output model – so called *SP* – which maps the temporally and spatially correlated daily multi-site *DNI* data into daily multi-site *CSP* power outputs. To deal with the uncertainty, variability and intermittency effects of multi-site *DNI* data, we utilized the insights we gained to develop the multi-site *DNI* model that probabilistically represents the multi-site *DNI* data. We made use of the *SP* and the multi-site *DNI* model to obtain the probabilistic characterization of the multi-site *CSP* power outputs, which we integrated into the extended probabilistic production simulation tool for systems with the multi-site *CSP* resources. We selected representative simulation results to illustrate the influences of multi-site *CSP* integration on the system variable effects for a wide variety of parametric studies. Our work provides

valuable insights into the role that multi-site *CSP* resources can play in the effective harnessing of solar energy and the utilization of *TES* in the deployment of such resources.

The extension of the probabilistic simulation approach to incorporate the representation of uncertain, time-varying *CSP* resources constitutes a significant improvement in the capability to emulate systems with variable energy resources. The capability to quantify the impacts of *CSP* resources on the economics of electricity supply, the emissions and the system reliability effects make the extended approach very useful for planning, investment decision, regulatory filing, and policy analysis applications. Our illustrative examples demonstrate the ability of the approach to answer a broad range of *what-if* questions on power systems with integrated multi-site *CSP*s.

5.2. Future Research

The proposed extension to the conventional production simulation approach is a good basis to develop a comprehensive simulation framework to evaluate the variable effects of systems with integrated *CSP* and wind resources at distinct sites. In addition, we can make use of the extended simulation tool to investigate the impacts of different *TES* operational objectives on the *CSP* contribution to power systems. We can also explore the stochastic simulation of systems with integrated *CSP* resources with the explicit representation of the day-ahead markets. Indeed, the advantages of the regime-based approach to capture both the seasonal and diurnal variability of the time-dependent resources can be exploited in other areas. We will report on such efforts in future publications.

APPENDIX A: NOTATION

S	number of *CSP* sites
s	subscript to denote the *CSP* site index with $s = 1, 2, \ldots, S$
H	number of smallest, indecomposable sub-periods from midnight to midnight in each day in the production simulation framework
h	the index of the smallest, indecomposable sub-period with $h = 1, 2, \ldots, H$
Δ_H	duration of the sub-period in the production simulation framework, computed by the ratio of 24 to H
c_s	*CSP* nameplate capacity in MW
$\beta_s(\cdot)$	nonlinear mapping of the *DNI* into the solar field thermal power output
$\alpha_s(\cdot)$	nonlinear mapping of the thermal energy flow rate into the *CSP* power output in MW
$k_s^d[h]$	rate of charge of thermal energy into the *TES* in MW_t
$v_s^d[h]$	*TES* charging state status variable $\in \{0, 1\}$
$q_s^d[h]$	rate of discharge of thermal energy from the *TES* in MW_t
$\varphi_s^d[h]$	*TES* discharging state status variable $\in \{0, 1\}$
$\varepsilon_s^d[h]$	thermal energy stored in the *TES* in MWh_t
$z_s^d[h]$	flow rate of thermal energy in MW_t to used for electricity generation
$\gamma_s^d[h]$	objective function coefficient in the scheduling optimization
$\varepsilon_s^{min}, \varepsilon_s^{max}$	lower, upper bound on the *TES* capability in MWh_t

k_s^{min}, k_s^{max} lower, upper bound on the *TES* charging capacity in $\mathrm{MW_t}$

η_s *TES* charging efficiency $\in (0, 1]$

q_s^{min}, q_s^{max} lower, upper bound on the *TES* rate of discharge of thermal energy in $\mathrm{MW_t}$

μ_s *TES* discharging efficiency $\in (0, 1]$

ψ_s *TES* thermal energy loss factor $\in [0, 1]$

z_s^{min}, z_s^{max} lower, upper bound on the rate of thermal energy delivery for electricity generation in $\mathrm{MW_t}$

I number of days in a seasonal *DNI* data collection

i superscript to denote the day index of the *DNI* measurements with $i = 1, 2, \ldots, I$

M_s^i number of *DNI* measurements collected from each equal-duration sub-period from sunrise to sunset

m index of the sub-period with $m = 1, 2, \ldots, M_s^i$

M number of equal-duration sub-periods from midnight to midnight with the identical time resolution as used for the *DNI* measurements

J number of time-scaled sub-periods in the sunrise-to-sunset period

j index of the time-scaled sub-period with $j = 1, 2, \ldots, J$

R number of identified *DNI* clusters

r subscript to denote the index of the identified *DNI* cluster with $r = 1, 2, ..., R$

$\mathcal{R}_r$ *DNI* cluster r

π_r probability of the *DNI* cluster $\mathcal{R}_r$

$\mathscr{R}_r$ *DNI* regime r

d superscript to denote the index of the day in the year for a specified season

$\hat{u}_s^i[m]$ *DNI* measurement for the sub-period m

$\underline{\hat{\boldsymbol{u}}}_s^i$ vector $\left[\hat{u}_s^i[1],\ \hat{u}_s^i[2],\ \ldots\ ,\ \hat{u}_s^i\left[M_s^i\right]\right]^T \in \mathbb{R}^{M_s^i}$

$y_s^i[j]$ computed common-time-scaled *DNI* value used in the clustering analysis

$\underline{\boldsymbol{y}}_s^i$ vector $\left[y_s^i[1],\ y_s^i[2],\ \ldots\ ,\ y_s^i[J]\right]^T \in \mathbb{R}^J$

$\underline{\bar{\boldsymbol{Y}}}^i$ array $\left[\underline{\boldsymbol{y}}_1^i \vdots\ \underline{\boldsymbol{y}}_2^i \vdots\ \ldots \vdots\ \underline{\boldsymbol{y}}_S^i\right] \in \mathbb{R}^{J\times S}$

$\hat{t}_s^{d,b}, \hat{t}_s^{d,e}$ actual sunrise, sunset time

$h_s^{d,b}, h_s^{d,e}$ sub-period that satisfies $max\{h : h\Delta_H \le \hat{t}_s^{d,b}\},\ min\{h : h\Delta_H \ge \hat{t}_s^{d,e}\}$

$t_s^{d,b}, t_s^{d,e}$ sunrise, sunset time determined by $t_s^{d,b} = h_s^{d,b}\Delta_H, t_s^{d,e} = h_s^{d,e}\Delta_H$

$\underset{\sim}{U}_s^d[h]$ sub-period h *DNI r.v.*

$\underset{\sim}{U}_s^d[h]\big|_r$ sub-period h *DNI r.v.* conditioned on the cluster $\mathscr{R}_r$

$\underline{\underset{\sim}{U}}_s^d$ *DNI r.v.* vector

$\underline{\underset{\sim}{U}}_s^d\big|_r$ *DNI r.v.* vector conditioned on the cluster $\mathscr{R}_r$

$\underline{\bar{\underset{\sim}{U}}}^d$ *DNI r.v.* array

$\underline{\bar{\underset{\sim}{U}}}^d\big|_r$ *DNI r.v.* array conditioned on the cluster $\mathscr{R}_r$

$u_s^d[h]$ sub-period h computed *DNI* value obtained from a random sample

$\underline{\boldsymbol{u}}_s^d$ vector $\left[u_s^d[1],\ u_s^d[2]\ \ldots\ ,\ u_s^d[H]\right]^T \in \mathbb{R}^H$

$\underset{\sim}{P}_s^d[h]$ sub-period h *CSP* power output *r.v.*

$\underset{\sim}{P}_s^d[h]\big|_r$ sub-period *h CSP* power output *r.v.* conditioned on the cluster $\mathcal{R}_r$

$p_s^d[h]$ sub-period *h CSP* power output

$\underline{\boldsymbol{p}}_s^d$ vector $\left[p_s^d[1],\ p_s^d[2],,\ \ldots\ ,\ p_s^d[H]\right]^T \in \mathbb{R}^H$

W number of the simulation periods in the study period

w index of the simulation period with $w = 1, 2, \ldots, W$

$\mathcal{T}$ index set of the sub-periods in the simulation period w

$\mathcal{E}$ index set of the conventional generation units

$\mathcal{E}^w$ index set of the committed conventional units in the simulation period w

$\underset{\sim}{L}$ load *r.v.*

$\underset{\sim}{L}\big|_h$ load *r.v.* conditioned on sub-period *h*

$\underset{\sim}{L}_k$ "remaining" load be served by the blocks of units in the loading list after the first $(k-1)$ blocks are loaded

$\mathcal{L}_k$ complement of the *c.d.f.* – the so-called load duration curve (*l.d.c.)* – of $\underset{\sim}{L}_k$

$\underset{\sim}{C}$ controllable load *r.v.*

Δ_J ratio of M_s^i to J

APPENDIX B: THE SCALING ALGORITHM

The scaling process is essential to undertake the comparison of the computed *DNI* data in a meaningful way. We present the scaling algorithm and state the general expression to compute $\underline{\boldsymbol{y}}_s^i$ from $\hat{\underline{\boldsymbol{u}}}_s^i$. We also provide an illustrative example.

We start out with a statement of the scaling algorithm:

Step B0: Define $\Delta_J = \frac{M_s^i}{J}$; initialize $\underline{\boldsymbol{y}}_s^i = \underline{\mathbf{0}}$; set $\tau = 0$, $j = 1$ and $m = 1$.

Step B1: If $m \le j\Delta_J$, set $y_s^i[j] = y_s^i[j] + \hat{u}_s^i[m](m - \tau)$ and $\tau = m$ and continue; else, go to step B3.

Step B2: If $m = M_s^i$, go to step B4; else, $m = m + 1$ and go to step B1.

Step B3: Set $y_s^i[j] = y_s^i[j] + \hat{u}_s^i[m]\left(j\Delta_J - \tau\right)$ and $\tau = j\Delta_J$ and compute $y_s^i[j] = \frac{y_s^i[j]}{\Delta_J}$.

Step B4: If $j = J$, stop; else, set $j = j + 1$ and go to step B1.

The scaling algorithm may be used to derive the explicit expression for the determination of $y_s^i[j]$ in the day *i* at the site *s*:

$$y_s^i[j] = \frac{1}{\Delta_J}\left\{\begin{array}{l} \sum_{m \in \mathcal{M}_1} y_s^i[m]\left(m - (j-1)\Delta_J\right) + \\ \sum_{m \in \mathcal{M}_0 / \left(\mathcal{M}_1 \cup \mathcal{M}_2\right)} y_s^i[m] + \sum_{m \in \mathcal{M}_2} y_s^i[m]\left(j\Delta_J - m\right) \end{array}\right\} \qquad \text{(B.1)}$$

where

$$\mathcal{M}_0 = \{\, m : (j-1)\Delta_J \le m < j\Delta_J \,,\ 1 \le m \le M_s^i \,\}$$
$$\mathcal{M}_1 = \{\, m : (m-1) < (j-1)\Delta_J \le m \,,\ 1 \le m \le M_s^i \,\}$$
$$\mathcal{M}_2 = \{\, m : m \le (j+1)\Delta_J < (m+1) \,,\ 1 \le m \le M_s^i \,\}$$
$$\mathcal{M}_0 / (\mathcal{M}_1 \cup \mathcal{M}_2) = \{\, m : m \in \mathcal{M}_0 \,,\ m \notin \mathcal{M}_1 \text{ and } m \notin \mathcal{M}_2 \,\}.$$

We illustrate the scaling process graphically in Fig. B.1. The value of $y_s^i[j]$ is determined in terms of the area under the step function for the measured *DNI* values, constructed from $\underline{\hat{u}}_s^i$, over the duration that corresponds to the common time scale sub-period j.

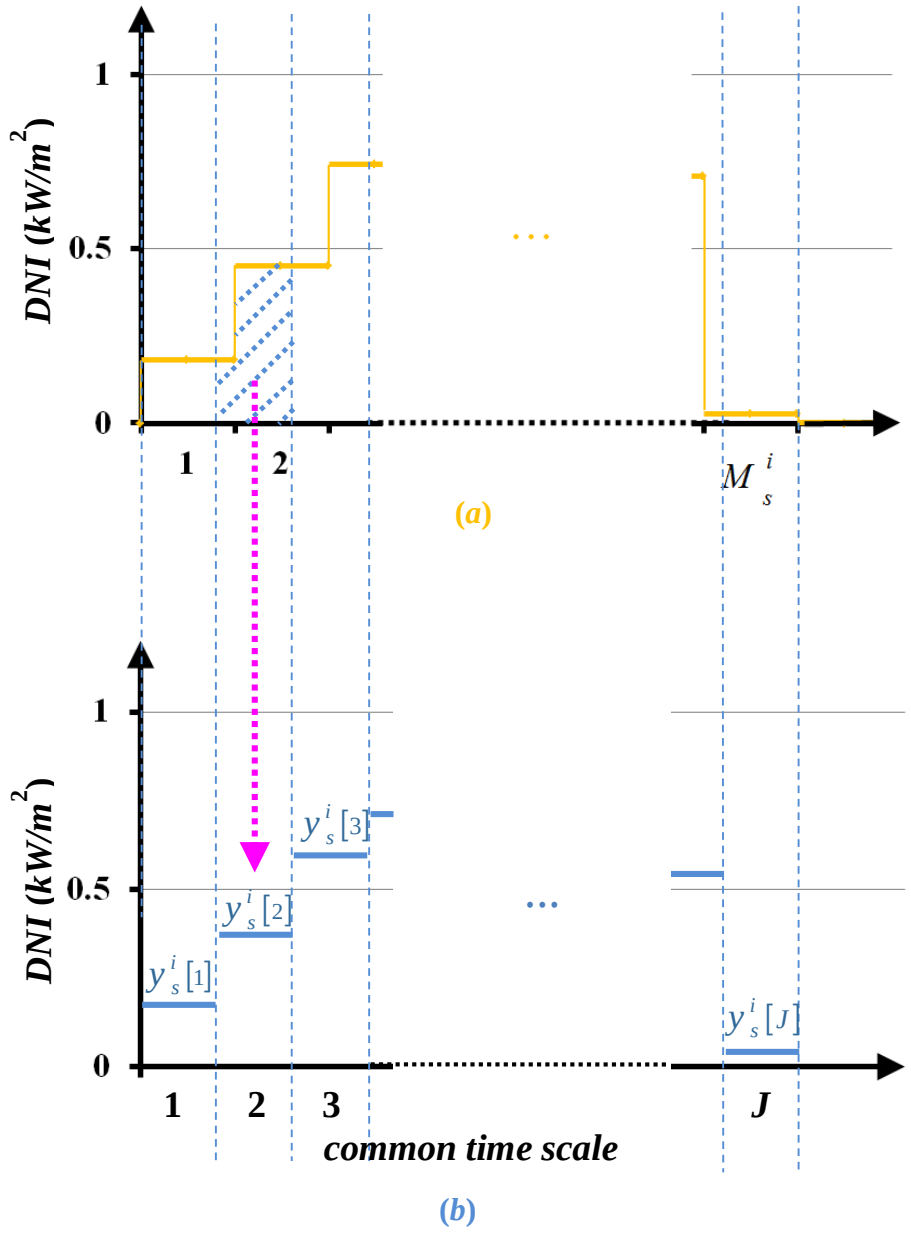

Figure B.1. The scaling process uses the measured values of the M_s^i sub-periods in the sunrise-to-sunset period to obtain the common time scale sub-period j computed value $y_s^i[j]$, j=1, 2, …, J

APPENDIX C: THE DESCALING ALGORITHM

The descaling process is essential in the determination of the computed *DNI* data in the common time scale for a given day *d*. We present a statement of the descaling algorithm and derive a formula for the determination of the *DNI* value $u_s^d[h]$ for each sub-period *h* such that $h_{b,s}^d \le h \le h_{e,s}^d$ in the day *d* at the site *s*. We also illustrate the application of the algorithm with a graphical example.

We start out with a statement of the scaling algorithm:

Step C0: Define $\Delta_H = \frac{24}{H}, \Delta_J = \frac{t_s^{d,e} - t_s^{d,b}}{J}$; initialize $\underline{\boldsymbol{u}}_s^d = \underline{\mathbf{0}}$; set $h_s^{d,b} = \frac{t_s^{d,b}}{\Delta_H}$ and $h_s^{d,e} = \frac{t_s^{d,e}}{\Delta_H}$; set $\tau = h_s^{d,b}$, $j = 1$ and $h = h_s^{d,b}$.

Step C1: If $t_s^{d,b} + j\Delta_J \le h\Delta_H$, set $u_s^d[h] = u_s^d[h] + y_s^i[j]\left(t_s^{d,b} + j\Delta_J - \tau\right)$ and set $\tau = t_s^{d,b} + j\Delta_J$, continue; else, go to step C3.

Step C2: If $j = J$, go to step C4; else, set $j = j + 1$, go to step C1.

Step C3: Set $u_s^d[h] = u_s^d[h] + y_s^i[j]\left(h\Delta_H - \tau\right)$ and $\tau = h\Delta_h$ and $u_s^d[h] = \frac{u_s^d[h]}{\Delta_H}$.

Step C4: If $h = h_s^{d,e}$, stop; else, set $h = h + 1$ and go to step C2.

The steps above provide the basis for the explicit expression to determine $u_s^d[h]$ for each *h* that satisfies $h_s^{d,b} \le h \le h_s^{d,e}$ in the day *d* at the site *s*. We can show that:

$$u_s^d[h] = \frac{1}{\Delta_H}\left\{ \begin{array}{c} \sum_{j \in \mathcal{J}_1} y_s^i[j]\left(t_s^{d,b} + j\Delta_J - (h-1)\Delta_H\right) + \sum_{j \in \mathcal{J}_2} y_s^i[j]\left(h\Delta_1 - \left(t_s^{d,b} + j\Delta_J\right)\right) \\ \sum_{j \in \mathcal{J}_0 / \left(\mathcal{J}_1 \cup \mathcal{J}_2\right)} y_s^i[j]\Delta_j + \sum_{j \in \mathcal{J}_2} y_s^i[j]\left(h\Delta_H - t_s^{d,b} - j\Delta_J\right) \end{array} \right\} \qquad \text{(C.1)}$$

where

$$\mathcal{J}_0 = \{\ j : (h-1)\Delta_H \le t_s^{d,b} + j\Delta_J < h\Delta_H + \Delta_J\ ,\ 1 \le j \le J\ \}$$
$$\mathcal{J}_1 = \{\ j : t_s^{d,b} + (j-1)\Delta_J < (h-1)\Delta_H \le t_s^{d,b} + j\Delta_J\ ,\ 1 \le j \le J\ \}$$
$$\mathcal{J}_2 = \{\ j : t_s^{d,b} + j\Delta_J \le h\Delta_H + \Delta_J < t_s^{d,b} + (j+1)\Delta_J\ ,\ 1 \le j \le J\ \}$$
$$\mathcal{J}_0 / (\mathcal{J}_1 \cup \mathcal{J}_2) = \{\ j : j \in \mathcal{J}_0\ ,\ m \notin \mathcal{J}_1 \text{ and } m \notin \mathcal{J}_2\ \}.$$

Rather than provide a proof of (C.1), we illustrate the de-scaling process graphically. In the descaling algorithm, we "extend" or "compress" the common-time-scaled *DNI* vector $\underline{\boldsymbol{y}}_s^i$, as seen in Fig. C.1 (*a*), into the actual sunrise-to-sunset period of the day *d* at the site *s*. However, in the discrete-time representation of the $\underline{\boldsymbol{u}}_s^d$, the actual sunrise (sunset) need not precisely occur at the start or end of a sub-period. However, in our representation, we assume the sunrise occurs precisely at the start of the sub-period during which the sun rises. Similarly, we also assume the sunset occurs precisely at the end of the sub-period during which the sun sets. The value of $u_s^d[h]$ is determined by the area under the step function constructed from the values in $\underline{\boldsymbol{y}}_s^i$, for the sub-period *h*. We compute the *DNI* value $u_s^d\left[h_{b,s}^d + 1\right]$, as shown in Fig. C.1 (*b*) and (c).

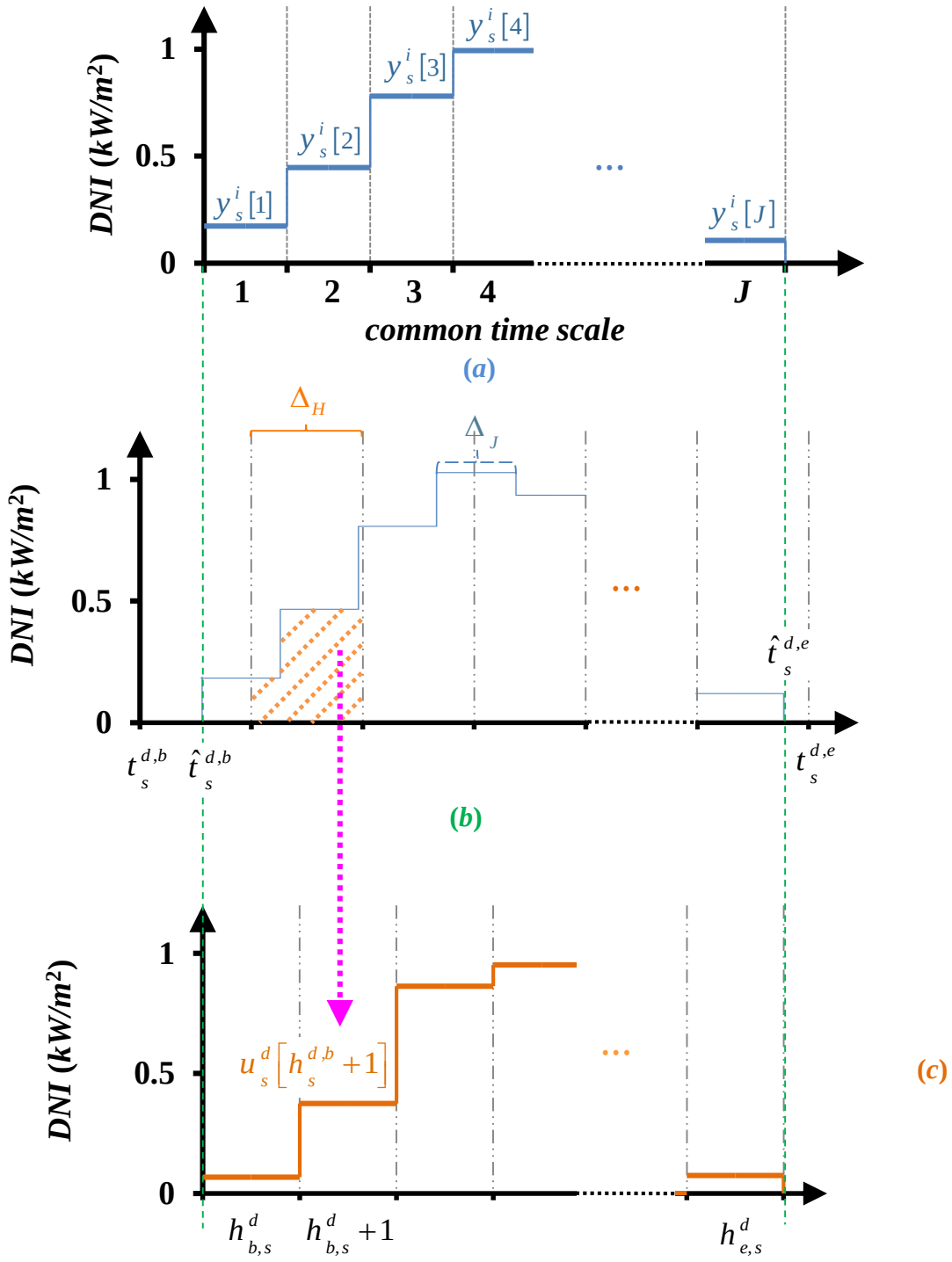

Figure C.1. The value of the $u_s^d[h]$ in (*c*) is obtained the common-time scale values in (*a*) with specific illustration of the value $u_s^d\left[h_s^{d,b}+1\right]$ as indicated in (*b*)

REFERENCES

[1] DSIRE—Database of State Incentives for Renewables & Efficiency. [Online]. Available: http://www.dsireusa.org/.

[2] P. Brown, "European Union wind and solar electricity policies: overview and considerations," 2013. [Online]. Available: https://www.fas.org/sgp/crs/row/R43176.pdf.

[3] Concentrating Solar Power Projects. [Online]. Available: http:// www.nrel.gov /csp.

[4] U. Wang, "The rise of concentrating solar thermal power," 2011. [Online]. Available: http://www.renewableenergyworld.com/rea/news/article/2011/06/the-rise-of concentrating-solar-thermal-power.

[5] IRENA, "Concentrating solar power," *Renewable Energy Technologies: Cost Analysis Series*, vol.1, no.2, Jun.2012.

[6] CSP Alliance, "The economic and reliability benefits for csp with thermal energy storage." [Online]. Available: http://www.csp-alliance.org/updated-cspa-report-september-2014/.

[7] MIDC – Measurement and Instrumentation Data Center [Online]. Available: http:// www.nrel.gov/midc/.

[8] Sunrise Sunset Calendar [Online]. Available: http:// www. sunrisesunset.com/usa.

[9] CAISO, "Reports and data," 2014, California Independent System Operator, Folsom, CA. [Online]. Available: http://www.caiso.com/market/Pages/ReportsBulletins/Daily RenewablesWatch.aspx.

[10] M. Masters, *Renewable and Efficient Electric Power Systems*, second edition, John Wiley & Sons Inc., Hoboken, NJ, 2013.

[11] T. Soubdhan et al., "Classification of daily solar radiation distributions using a mixture of Dirichlet distributions," *Solar Energy*, vol. 83, no. 7, pp. 1056-1063, July 2009.

[12] E. Lorenz et al., "Irradiance forecasting for the power prediction of grid-connected photovoltaic systems," *IEEE Journal of Selected Topics in Applied Earth Observations and Remote Sensing*, vol. 2, no. 1, pp. 2-10,Jan. 2009.

[13] S. Madaeni et al., "Estimating the capacity value of concentrating solar power plants: A case study of the southwestern United States," *IEEE Trans. Power Syst.*, vol. 27, no. 2, pp.1116–1124, May 2012.

[14] R. Sioshansi and P. Denholm, "The value of concentrating solar power and thermal energy storage," *IEEE Trans. Sustain. Energy*, vol. 1, no. 3, pp. 173–183, Oct. 2010.

[15] R. Dominguez et al., "Optimal offering strategy for a concentrating solar power plant," *Applied Energy*, vol. 98, pp.316-325, 2012

[16] Y. Zhang and S. Smith, "Long-term modeling of solar energy: analysis of concentrating solar power (CSP) and PV technologies," 2011. [Online]. Available: http://www.pnl.gov/main/ publications/external/technical_reports/pnnl-16727.pdf

[17] D. Halamay and K. Ted, "Monte Carlo analysis of the impacts of high renewable power penetration," in 2011 IEEE Energy Conversion Congress and Exposition (ECCE), Sep. 2011, pp. 3059-3066.

[18] J. Price and J. Goodin, "Reduced network modeling of WECC as amarket design prototype," in Proceedings of the IEEE PES General Meeting, Detroit, July 24-28 2011, pp. 1-6.

[19] M. Milligan, "Methods to model and calculate capacity contributions of variable generation for resource adequacy planning (IVGTF1-2): Additional discussion," National Renewable Energy Laboratory, Atlanta, GA, Tech. Rep., Jan. 2011.

[20] A. Wood, B. Wollenberg and G. Sheblé, *Power Generation, Operation and Control*, John Wiley & Sons Inc., Hoboken, NJ, 2013.

[21] S. Karaki et al., "Probabilistic performance assessment of autonomous solar-wind energy conversion systems," *IEEE Trans. Energy Convers.*, vol. 14, no.3, pp. 766–772, Sept. 1999.

[22] NREL, "Solar Advisor Model," 2012, National Renewable Energy Laboratory, Golden, CO. [Online]. Available: https://sam.nrel.gov/.

[23] A. Rovira et al., "Energy management in solar thermal power plants with double thermal storage system and subdivided solar field," *Applied Energy*, vol.88, no.11, pp. 4055-4066, Nov. 2011.

[24] J. Usaola, "Operation of concentrating solar power plants with storage in spot electricity markets," *IET. Renewable Power Generation*, vol. 6, no.1, pp. 59-66, Jan. 2012.

[25] K. Powell and T. Edgar, "Modeling and control of a solar thermal power plant with thermal energy storage," *Chemical Engineering Science*, vol. 71, pp. 138-145, Mar. 2012.

[26] R. Bhana, "A production simulation tool for systems with integrated photovoltaic energy resources." Dept. Elect. & Comput. Eng. Univ. Illinois, Urbana-Champaign, 2011.

[27] R. Xu and D. Wunsch, "Partitional clustering", in *Clustering,* John Wiley & Sons Inc., Hoboken, NJ, pp. 67-72, 2009.

[28] N. Maisonneuve and G. Gross, "A production simulation tool for systems with integrated wind energy resources," *IEEE Trans. Power Syst*., vol. 26, no. 4, pp. 2285-2292, Nov. 2011.

[29] G. Gross, "Electricity Resource Planning," class notes for ECE 588, Dept. Elect. & Comput. Eng. Univ. Illinois, Urbana-Champaign, Fall 2012.

[30] J. Price and J. Goodin, "Reduced network modeling of WECC as a market design prototype," in Proceedings of the IEEE PES General Meeting, Detroit, July 24-28 2011, pp. 1-6.

[31] NOAA, "Climate data for stations," National Oceanic and Atmospheric Administration, Silver Spring, MD. [Online]. Available: http://www7.ncdc.noaa.gov/CDO/dataproduct.

[32] Y. Degeilh and G. Gross, "Stochastic simulation of power systems with integrated intermittent renewable resources," submitted to *IEEE Trans. on Power Systems*.